



Review

Structure and electronic properties of Pd(III) complexes

Liviu M. Mirica*, Julia R. Khusnutdinova

Department of Chemistry, Washington University, One Brookings Drive, St. Louis, MO 63130-4899, United States

Contents

1. Introduction	299
2. Mononuclear Pd(III) complexes	300
2.1. Pd(III) coordination compounds	300
2.2. Organometallic Pd(III) complexes	303
3. Dinuclear Pd(III) complexes	305
3.1. Dinuclear Pd(II) precursors	305
3.2. Mixed-valent Pd ^{II} /Pd ^{III} complexes	305
3.3. Dinuclear Pd(III) complexes with a Pd–Pd bond	307
3.4. Dinuclear Pd(III) complexes without a Pd–Pd bond	309
4. Summary and outlook	313
Acknowledgments	313
References	313

ARTICLE INFO

Article history:

Received 22 February 2012
 Received in revised form 5 April 2012
 Accepted 23 April 2012
 Available online 30 April 2012

Dedicated to Professor Edward Solomon on the occasion of his 65th birthday.

Keywords:

Mononuclear Pd(III) complexes
 Dinuclear Pd(III) complexes
 Pd catalysis
 EPR
 Chemical oxidation
 Electrolysis

ABSTRACT

Despite the rich chemistry of palladium in oxidation states of 0, +2, and +4, no Pd^{III} coordination compounds have been reported until the 1980s. Moreover, while Pd complexes are among the most commonly used catalysts in organometallic chemistry, the first organometallic Pd^{III} complexes have only been reported in 2006. Since then, a significant number of Pd^{III} complexes have been isolated, characterized, and proposed as active catalytic intermediates in the functionalization of C–H bonds, oxidatively induced C–C bond formation reactions, as well as radical insertion and addition reactions. This review provides an overview of the synthesis and spectroscopic characterization of mononuclear and dinuclear Pd^{III} complexes. A detailed understanding of the steric and electronic properties of Pd^{III} complexes should provide insight for the development of novel catalysts for multi-electron redox reactions and various organometallic transformations.

© 2012 Elsevier B.V. All rights reserved.

1. Introduction

Palladium is one of the most catalytically versatile transition metals, its complexes being efficient catalysts for a wide range of C–C coupling, C–H functionalization, and hydrocarbon oxidation reactions [1–3]. For example, the 2010 Nobel Prize in Chemistry was awarded for palladium-catalyzed cross-coupling reactions [4]. While Pd can exist in five oxidation states (0, +1, +2, +3, and +4) [5], the vast majority of Pd-catalyzed reactions involve Pd⁰ and Pd^{II} oxidation states and these transformations have been extensively

investigated for the past several decades [2,6–9]. In addition, Pd^{IV} complexes have been reported starting more than two decades ago [10–19], and have been shown recently to be involved in a variety of Pd-catalyzed ligand-directed C–H oxidative functionalization reactions [20–26]. By comparison, complexes of odd-electron Pd^I and Pd^{III} oxidation states are much less common. Several dinuclear Pd^I complexes stabilized by a Pd–Pd bond have been reported [27–33], however, no mononuclear Pd^I complexes have been isolated to date [34]. Herein, we provide an overview of the synthesis and spectroscopic characterization of mononuclear and dinuclear Pd^{III} complexes. Dinuclear Pd^{III} complexes have been proposed recently as active catalytic intermediates in the oxidative functionalization of C–H bonds [35–39] and aza-Claisen rearrangements [40], while mononuclear Pd^{III} complexes have been proposed as

* Corresponding author. Tel.: +1 314 935 3464; fax: +1 314 935 4481.
 E-mail address: mirica@wustl.edu (L.M. Mirica).

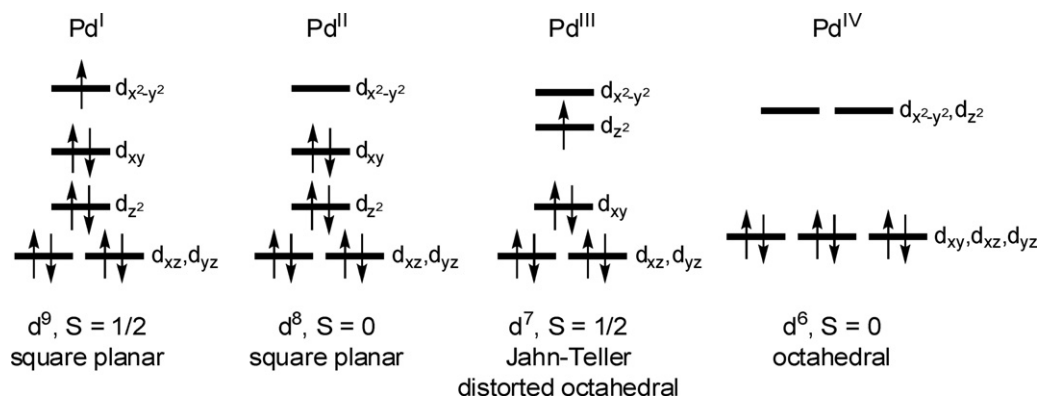


Fig. 1. Representative d electron configuration of Pd^I, Pd^{II}, Pd^{III}, and Pd^{IV} oxidation states. For square planar geometry, the energy ordering of the d_{z^2} and d_{xz}/d_{yz} orbitals can vary depending on the ligand field strength [47].

transient intermediates in oxidatively induced reductive elimination of ethane from Pd^{II}Me₂ complexes [41–43], the insertion of dioxygen into a Pd–Me bond [44], Kumada coupling [45], and the Kharasch reaction [46]. In this context, a detailed understanding of the steric and electronic properties of Pd^{III} complexes should provide insight into the development of novel catalysts for various organometallic transformations as well as other multi-electron redox reactions.

2. Mononuclear Pd(III) complexes

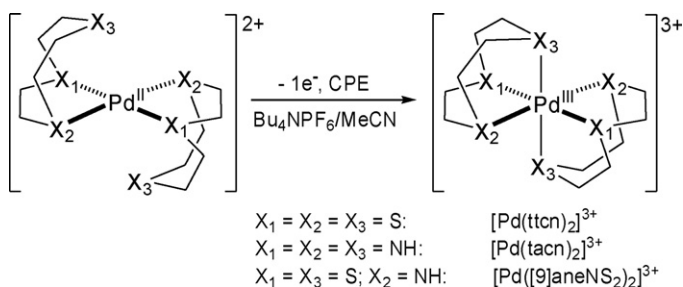
The Pd oxidation states of +1, +2, +3, and +4 correspond to d^9 , d^8 , d^7 , and d^6 electron configurations, respectively (Fig. 1). Pd^I complexes exhibit square planar d^9 metal centers, although a square pyramidal geometry can also be envisioned by analogy to Cu^{II} systems. Pd^{II} d^8 complexes almost exclusively exhibit a square planar geometry with the highest occupied molecular orbital (HOMO) being the Pd-based d_{z^2} orbital [47], although a triplet ground state can also be possible [48,49]. One-electron oxidation of these Pd^{II} systems leads to formation of paramagnetic, Pd^{III} d^7 centers that prefer a Jahn–Teller distorted octahedral geometry. By comparison, a symmetric octahedral geometry is generally observed for the Pd^{IV} d^6 centers (Fig. 1).

2.1. Pd(III) coordination compounds

Initial attempts to synthesize Pd^{III} complexes have focused on binary fluoride compounds with the PdF₃ empirical formula [50]. These compounds exhibited a magnetic moment corresponding to one unpaired electron per Pd, suggestive of Pd^{III} centers [50,51]. However, later studies have shown that these binary fluorides are better described as Pd²⁺[PdF₆]²⁻, in which the Pd²⁺ ion exhibits a high spin electron configuration with two unpaired electrons due to the weak-field fluoride anions and the Pd⁴⁺ has a low spin, diamagnetic configuration [48,49]. The first genuine Pd^{III} compound, NaPdF₄, was obtained in 1982 by solid-state synthesis from NaF and Pd₂F₆ at high pressure and temperature [52]. The Pd^{III} oxidation state has been unambiguously confirmed by the presence of an axial EPR spectrum with $g_{\parallel} = 2.0504$ and $g_{\perp} = 2.263$ that suggests the presence of an unpaired electron in the d_{z^2} orbital [53], in line with the Jahn–Teller axial elongation of the coordination geometry and the observed monoclinic unit cell. Additional elpasolite-type Pd compounds of A₂BPdF₆ formulation (A, B: alkali metals) have been reported to contain Pd^{III} centers with a doublet ground state, as confirmed by EPR spectroscopy and magnetic measurements [54–58]. In general, these compounds exhibit axial EPR spectra due to a Jahn–Teller tetragonal distortion – with g_{\parallel} and g_{\perp} values of 2.01–2.05 and 2.28–2.31, respectively, although both rhombic and

isotropic EPR spectra have also been observed (Table 1). The degree of anisotropy and presence of isotropic signals at higher temperatures have been related to changes from a static to a dynamic Jahn–Teller distortion [56].

The first structurally characterized Pd^{III} coordination compound that exists both in solution and the solid state is the homoleptic 1:2 adduct with the tridentate macrocyclic ligand 1,4,7-trithiacyclononane, ttcn, reported in 1987 by Schröder and co-workers [59]. The cyclic voltammetry of the Pd^{II} complex [Pd^{II}(ttcn)₂]²⁺ shows a reversible oxidation wave at +0.605 V vs. Fc/Fc⁺ in MeCN solution assigned to a Pd^{II/III} oxidation. Oxidation of the Pd^{II} precursor [Pd^{II}(ttcn)]²⁺ by either controlled potential electrolysis (CPE) in MeCN or chemical oxidation with 70% HClO₄ affords an orange species with a visible transition at 476 nm (Scheme 1). The presence of a paramagnetic Pd^{III} center was confirmed by the EPR spectrum that shows an anisotropic signal with $g_{\parallel} = 2.009$ and $g_{\perp} = 2.049$ with partially discernible hyperfine couplings to ¹⁰⁵Pd (22.8% abundance, $I = 5/2$) of $A_{\perp} = 20$ G and $A_{\parallel} = 5$ G. Since the ttcn ligand exhibits an oxidation potential ~400 mV higher than that of [Pd^{II}(ttcn)]²⁺, the authors concluded that a metal-based oxidation process is predominant, although it was shown recently that the redox-active S donors contribute significantly to the singly occupied molecular orbital (SOMO) [60]. The X-ray structure of the isolated red crystals reveals a [Pd(ttcn)₂]³⁺ cation with a trigonally elongated octahedral geometry, in line with a Jahn–Teller distorted Pd^{III} d^7 center (Fig. 2a), with Pd–S_{ax} = 2.545 Å and average Pd–S_{eq} = 2.362 Å. An analogous homoleptic 1:2 Pd^{III} complex using the 1,4,7-triazacyclononane ligand, tacn, was reported by the same group in 1988 (Scheme 1) [61]. The corresponding [Pd(tacn)₂]²⁺ complex exhibits a much lower oxidation potential than [Pd(ttcn)₂]²⁺ (0.07 V compared to 0.60 V vs. Fc/Fc⁺, respectively), as expected for the presence of harder N donors (Table 1). In addition, CPE of [Pd(tacn)₂]²⁺ in MeCN generates a bright yellow [Pd(tacn)₂]³⁺



Scheme 1. Synthesis of Pd^{III} complexes supported by N- and/or S-donor tridentate macrocyclic ligands [59,61,65].

Table 1
Spectroscopic and electrochemical properties of mononuclear Pd^{III} complexes.

Complex	UV-vis, λ , nm (ϵ , M ⁻¹ cm ⁻¹)	Redox potentials (vs. Fc/Fc ⁺)	EPR, g_x, g_y, g_z (A values, G)	References
NaPdF ₄	ND	ND	$g_{\perp} = 2.263, g_{\parallel} = 2.0504^a$	[52]
Na ₃ PdF ₆	ND	ND	$g_{\perp} = 2.312, g_{\parallel} = 2.025^b$	[56]
Cs ₂ KPdF ₆	ND	ND	$g_x = 2.297, g_y = 2.197,$ $g_z = 2.012^b$	[56]
[(ttn) ₂ Pd] ³⁺ ttn = 1,4,7-trithiacyclononane	477 (5350), 341 (16,100), 230 (8100) ^c	$E_{1/2}^{II/III} = 0.605$ ($\Delta E_p = 84$ mV) ^{d,e}	$g_x = 2.046$ ($A_x^{Pd} = 25$ G), $g_y = 2.041$ ($A_y^{Pd} = 23$ G), $g_z = 2.004$ ($A_z^{Pd} = 15$ G) ^{f,g}	[59,60]
[(tacn) ₂ Pd] ³⁺ tacn = 1,4,7-triazacyclononane	383 (590), 314 (1240), 196 (11,200) ^c	$E_{1/2}^{II/III} = 0.07$ V, $E_{1/2}^{III/IV} \sim +0.45$ V ^{d,e} ($E_{1/2}^{II/III} = 0.37$ V, $E_{1/2}^{III/IV} = +0.64$ V vs. NHE) ^h	$g_{\perp} = 2.123,$ $g_{\parallel} = 2.007$ ($A_{\parallel}^N = 27$ G) ^{i,j}	[61,62]
[Pd([18]aneN ₂ S ₄)] ³⁺	488 (3180), 341 (5890), 264 (11,170) ^k	$E_{1/2}^{II/III} = 0.57$ V ($\Delta E_p = 195$ mV), $E_{pa}^{III/IV} = +1.30$ V (quasirev.) ^{d,e}	$g_x = 2.064, g_y = 2.052,$ $g_z = 2.019^i$	[63,64]
[Pd([9]aneNS ₂) ₂] ³⁺	245 (5400), 265 (9600), 328 (9000), 455 (5400) ^k	$E_{1/2}^{II/III} = 0.43$ V ($\Delta E_p = 140$ mV), $E_{1/2}^{III/IV} = +0.84$ V ($\Delta E_p = 130$) ^{d,e}	$g_{\perp} = 2.058, g_{\parallel} = 2.008^l$	[65]
[Pd([18]aneS ₆)] ³⁺	ND	ND	$g_x = 2.048$ ($A_x^{Pd} = 23$ G), $g_y = 2.036$ ($A_y^{Pd} = 22.1$ G), $g_z = 1.998$ ($A_z^{Pd} = 4.3$ G) ^{f,g}	[60]
[(N ₄)PdMeCl] ⁺	723 (1100), 545 (490), 368 (3300), 263 (12,000) ^k	$E_{pc}^{III/II} = -0.426$ V, $E_{pa}^{II/III} = +0.150$ V, $E_{1/2}^{III/IV} = +0.585$ V ($\Delta E_p = 68$ mV) ^d	$g_x = 2.239, g_y = 2.134,$ $g_z = 2.005$ ($A_N = 19.5$ G) ^l	[42,118]
[(N ₄)PdMe ₂] ⁺	741 (360), 350 (2300), 263 (10,300) ^k	$E_{pc}^{III/II} = -0.882$ V, $E_{pa}^{II/III} = -0.326$ V, $E_{1/2}^{III/IV} = +0.064$ V ($\Delta E_p = 62$ mV) ^d	$g_x = 2.222$ ($A_x^N = 12.0$ G), $g_y = 2.191$ ($A_y^N = 13.8$ G), $g_z = 1.986$ ($A_z^N = 18.0$ G) ^l	[43]
[(N ₄)PdPhCl] ⁺	732 (1100), 386 (2500), 258 (20,000) ^k	$E_{pc}^{III/II} = -0.022$ V, $E_{pa}^{II/III} = +0.368$ V, $E_{1/2}^{III/IV} = +0.708$ V ($\Delta E_p = 65$ mV) ^d	$g_x = 2.217, g_y = 2.131,$ $g_z = 2.003$ ($A_z^N = 21.4$ G) ^l	[42,118]
^m [PdCl ₅] ²⁻	ND	ND	$g_{\perp} = 2.149$ ($A_{\perp}^{Cl} = 10.8$ G), $g_{\parallel} = 2.012$ ($A_{\parallel}^{Cl} = 63.8$ G) ⁿ	[66]
^o [PdCl ₆] ³⁻	ND	ND	$g_{\perp} = 2.184$ ($A_{\perp}^{Cl} = 6.8$ G), $g_{\parallel} = 2.012$ ($A_{\parallel}^{Cl} = 38.2$ G)	[67]
Pd ³⁺ in CaO single crystal	ND	ND	$g_{\perp} = 2.221$ ($A_{\perp} = 6.6$ G), $g_{\parallel} = 2.011$ ($A_{\parallel} = 0.5$ G)	[72]
^p [Pd(CN) ₄ Cl ₂] ³⁻	ND	ND	$g_{\perp} = 2.1257$ ($A_{\perp}^{Cl} = 12.6$ G), $A_{\parallel}^{Pd} = 34.9$ G, $g_{\parallel} = 1.9967$ ($A_{\parallel}^{Cl} = 53.2$ G), $A_{\parallel}^{Pd} = 42.9$ G) ^q	[68]
[Pd(NH ₃) ₄] ^{3+r}	ND	ND	$g_{\perp} = 2.29, g_{\parallel} = 2.23^r$	[73]

ND: not determined.

^a 8 K.

^b 4.2 K.

^c In H₂O.

^d In nBu₄NPF₆/MeCN.

^e Determined for corresponding Pd^{II} complexes.

^f In HClO₄(aq), 50 K.

^g Superhyperfine coupling to four equivalent ¹H nuclei was also observed.

^h In 1 M LiClO₄(aq).

ⁱ In MeCN, 77 K.

^j Similar g values are observed in Li₂SO₄/H₂O, while an isotropic signal ($g_{iso} = 2.077$) is observed in H₂O.

^k In MeCN.

^l In PrCN–MeCN, 77 K.

^m Obtained by γ irradiation of K₂PdCl₄.

ⁿ Single crystal, 77 K.

^o Obtained by UV irradiation of Pd-doped AgCl crystals.

^p Obtained by X-ray irradiation of K₂[Pd(CN)₄]-doped KCl crystals.

^q Single crystal, 77 K.

^r Obtained by passing O₂ at 350 °C over Pd-doped Al₁₃-pillared montmorillonite.

^s Room temperature.

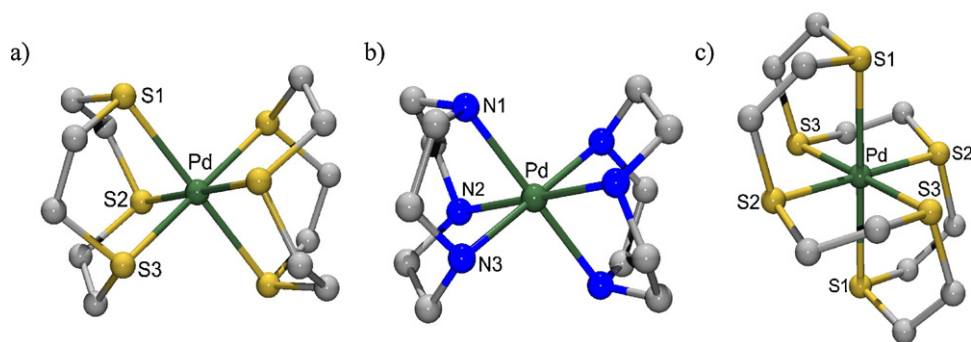


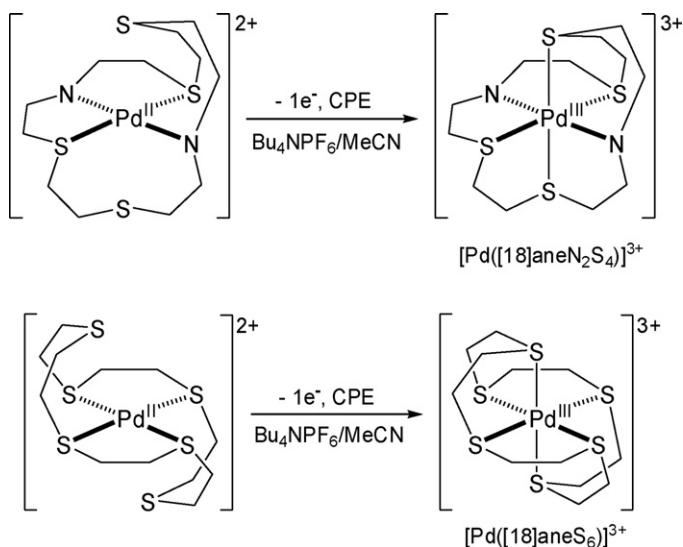
Fig. 2. Crystal structures of tricationic Pd^{III} complexes. Selected bond distances (Å): (a) [(ttcn)₂Pd^{III}]³⁺, Pd–S1 2.545, Pd–S2 2.356, Pd–S2 2.369 [59]; (b) [(tacn)₂Pd^{III}]³⁺, Pd–N1 2.180, Pd–N2 2.118, Pd–N3 2.111 [61]; (c) [(18)aneS6Pd]³⁺, Pd–S1 2.547, Pd–S2 2.349, Pd–S2 2.345 [60]. Counteranions are omitted for clarity.

species that is indefinitely stable in non-reducing solvents. The X-ray structure of the electrolysis product shows a Jahn–Teller distorted coordination around the Pd^{III} center with axial Pd–N_{ave} distances of 2.180 Å and equatorial Pd–N_{ave} of 2.115 Å (Fig. 2b), while its EPR spectrum reveals a nearly isotropic signal with $g_{\parallel} = 2.007$ and $g_{\perp} = 2.123$ and superhyperfine coupling to two N donors (a 1:2:3:2:1 quintet) with $A_{\parallel} = 27$ G. McAuley et al. have reported detailed EPR and electrochemical characterization of the same [Pd(tacn)₂]³⁺ species, showing the presence of a dynamic Jahn–Teller distortion at low ionic strengths that leads to loss of structure in the EPR spectrum; in addition, the spin–orbit coupling constant ($\lambda = 720$ cm^{−1}) and covalency parameter ($K = 0.66–0.72$) were determined for the Pd^{III} center based on experimental g values and the hyperfine coupling to ¹⁰⁵Pd [62]. Interestingly, the [Pd(tacn)₂]³⁺ species can be electrochemically oxidized to yield an unstable diamagnetic Pd^{IV} complex [61,62]. This Pd^{IV} species can react with [Pd(tacn)₂]²⁺ to yield the Pd^{III} species in a comproportionation reaction, a behavior that was also recently observed for other Pd^{III} systems (vide infra).

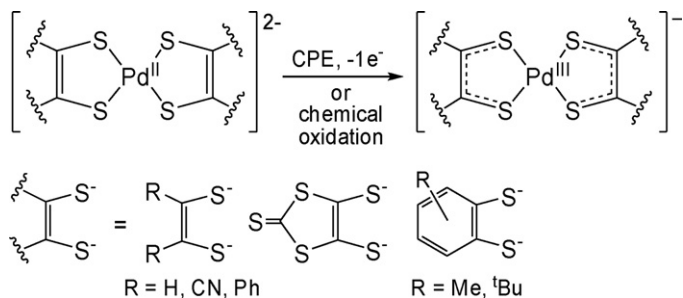
The two homoleptic 1:2 adducts described above suggest that formation of stable Pd^{III} complexes requires the presence of donor atoms in the axial positions of the metal center in order to stabilize the distorted octahedral geometry of the Pd^{III} d^7 metal center. This is supported by additional reports of macrocyclic ligands containing N and/or S donors that can accommodate the distorted octahedral geometry of the Pd^{III} center. For example, use of the hexadentate ligand [18]aneN₂S₄ leads to a bright-red Pd^{III} species that exhibits a rhombic EPR signal with unresolved hyperfine coupling to ¹⁰⁵Pd (Table 1, Scheme 2, top) [63,64]. The 1:2 adduct of Pd^{II} and [9]aneNS₂ (a mixed N,S-donor analog of ttcn and tacn, Scheme 1) generates upon one-electron oxidation an orange solution of [Pd([9]aneNS₂)₂]³⁺ that exhibits an axial EPR signal (Table 1). Superhyperfine coupling to N atoms is not observed for the latter species, suggesting that the N donors are bound in the equatorial plane (Scheme 1) [65]. In addition, it was recently reported that the hexathioether ligand [18]aneS₆ generates a stable dark-red Pd^{III} complex that was isolated and structurally characterized (Fig. 2c; Scheme 2, bottom), revealing UV–vis characteristics, EPR signals, and metrical parameters similar to the other Pd^{III}–macrocyclic complexes (Table 1). Interestingly, weak axial interactions with Pd–S_{ax} distances of 2.95–3.27 Å were observed in the X-ray structures of Pd^{II} precursors [Pd^{II}(ttcn)₂]²⁺, [Pd^{II}([9]aneNS₂)₂]²⁺, [Pd^{II}([18]aneN₂S₄)]²⁺, and [Pd^{II}([18]aneS₆)]²⁺, and these axial interactions may persist in solution and give rise to the visible transitions observed for the Pd^{II} precursors [59,60,63–65].

Several additional studies have reported the formation of Pd^{III} species in various coordination environments by irradiation [66–69] and electrochemical or chemical oxidation [70–75], and

the presence of Pd^{III} centers has been suggested based on EPR characterization (Table 1). For example, several Pd bis-dithiolene complexes have been reported to exhibit rhombic EPR signals assigned to presence of Pd^{III} species (Scheme 3, Table 1) [76–81]. However, the formation of a Pd^{II}–ligand radical species upon oxidation of Pd^{II} precursors needs also to be considered when redox non-innocent ligands (e.g., thiolate, phenolate, and phenylenediamine groups) are employed [82–84].



Scheme 2. Synthesis of Pd^{III} complexes supported by the hexadentate macrocyclic ligands [18]aneN₂S₄ [63] and [18]aneS₆ [60].



Scheme 3. Synthesis of “Pd^{III}” dithiolene and dithiolate complexes. These species are better described as Pd^{II}–ligand radical species (see text) [76–81].

2.2. Organometallic Pd(III) complexes

The first mononuclear organometallic Pd^{III} complexes were isolated and characterized by our group in 2010 (Scheme 4) [42]. In this study, the macrocyclic tetradentate ligand *N,N'*-di-*tert*-butyl-2,11-diaza[3.3](2,6)pyridinophane (N4) was employed to prepare the square planar Pd^{II} complexes (N4)Pd^{II}MeCl, (N4)Pd^{II}PhCl, and (N4)Pd^{II}Me₂. These complexes each exhibit two oxidation potentials that were assigned to Pd^{II}/Pd^{III} and Pd^{III}/Pd^{IV} couples, respectively (Fig. 3, Table 1). The Pd^{II}/Pd^{III} oxidation potentials are significantly lower than the oxidation potentials of analogous Pd^{II} complexes supported by bidentate N-donor ligands [41,43], and are likely due to the ability of the tetradentate ligand N4 to form tridentate (κ^3 -N4)Pd^{II} or tetradentate (κ^4 -N4)Pd^{II} species that have lower oxidation potentials [85–87], as well as stabilize the distorted octahedral geometry of the Pd^{III} center (Fig. 4) [42]. Due to these low oxidation potentials, facile one-electron electrochemical or chemical oxidation yields the dark-green Pd^{III} species [(N4)Pd^{III}MeCl]⁺, [(N4)Pd^{III}PhCl]⁺, and [(N4)Pd^{III}Me₂]⁺ (Scheme 4, top). Structural characterization of these stable complexes reveals tetragonally distorted octahedral geometries at the metal center, as expected for a Jahn–Teller distorted *d*⁷ Pd^{III} center (Fig. 4). The axial Pd–amine

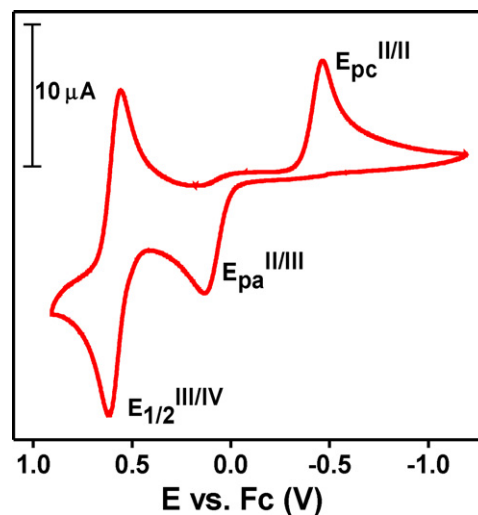


Fig. 3. Cyclic voltammogram of (N4)Pd^{II}MeCl in 0.1 M Bu₄NBF₄/CH₂Cl₂ (100 mV/s scan rate) [42]. Potentials vs. Fc/Fc⁺ (mV): $E_{pa}^{II/III} = +134$, $E_{pc}^{III/II} = -464$, $E_{1/2}^{III/IV}(\Delta E_p) = +587(63)$..

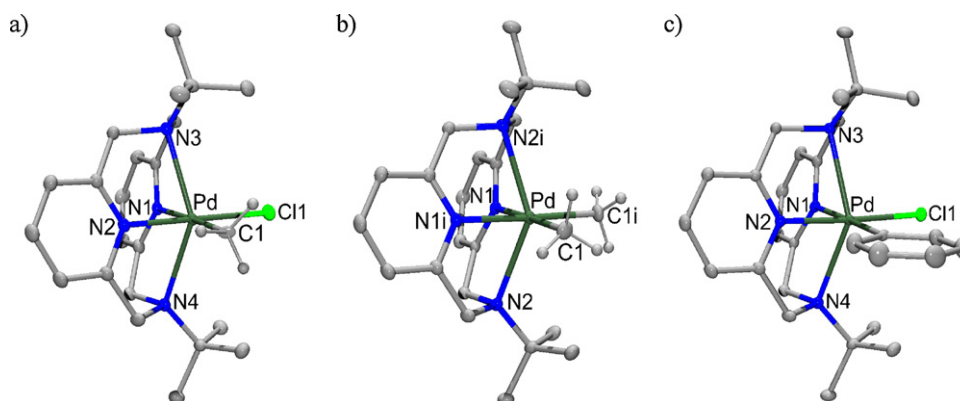
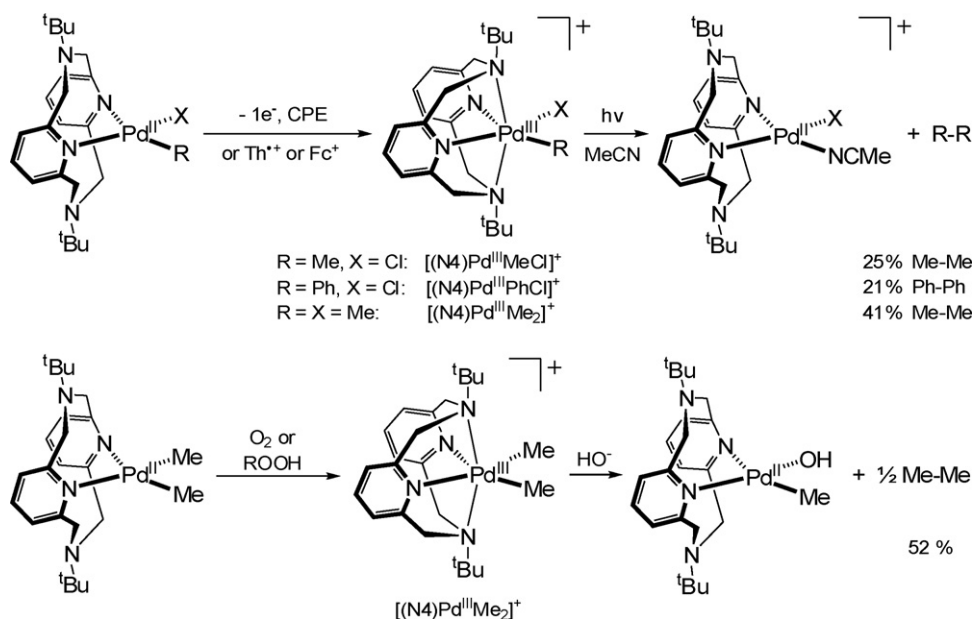


Fig. 4. Crystal structures of (N4)Pd^{III} complexes. Selected bond distances (Å): (a) [(N4)Pd^{III}MeCl]⁺, Pd–C1 2.092, Pd–Cl1 2.340, Pd–N1 2.097, Pd–N2 2.020, 2.427, Pd–N4 2.426 [42]; (b) [(N4)Pd^{III}Me₂]⁺ (from MeOH), Pd–C1 2.048, Pd–N1 2.112, Pd–N2 2.469, Pd–C1 2.092, Pd–Cl1 2.34, Pd–N1 2.097, Pd–N2 2.020, Pd–N3 2.427, Pd–N4 2.426 [43]; (c) [(N4)Pd^{III}PhCl]⁺, Pd–C(Ph) 2.071, Pd–Cl1 2.348, Pd–N1 2.093, Pd–N2 2.028, Pd–N3 2.424, Pd–N4 2.413 [42]. Counteranions and solvent molecules are omitted for clarity.



Scheme 4. Synthesis and reactivity (N4)Pd^{III} complexes (Th⁺: thianthrenyl cation radical; Fc⁺: ferrocenium) [42,43].

nitrogen bond distances (2.41–2.48 Å) are elongated compared to the equatorial Pd–pyridyl bond distances (2.02–2.11 Å). These complexes are paramagnetic and their EPR spectra exhibit signals with different anisotropies and $g_{\text{ave}} = 2.118\text{--}2.133$, suggesting a Pd^{III} center with a d_{z^2} ground state (Table 1 and Fig. 5) [42]. In addition, superhyperfine couplings to two N atoms ($A_{\text{N}} = 12\text{--}21$ G) are observed for one or more g values, while poorly defined hyperfine coupling to ¹⁰⁵Pd ($A \approx 44$ G) is present in the g_x/g_y direction. Interestingly, the EPR spectra of these complexes in a protic or glassing solvent mixture are different from the broad EPR spectra observed in MeCN [42,43]. This difference is likely due to a more symmetric structure of (N4)Pd^{III} species in a glassing or protic solvent that results in sharper EPR features and a larger separation between the g_z and g_x/g_y values [62]. In addition, the presence of a dynamic Jahn–Teller distortion in frozen MeCN at 77 K can also lead to broader EPR spectra [60,88].

The ability of the N4 ligand to stabilize Pd^{III} vs. Pd^{II} or Pd^{IV} complexes is intriguing and proposed to be due to the steric properties of the N4 ligand. While the axial nitrogens of this tetradentate ligand can coordinate and stabilize the Jahn–Teller distorted Pd^{III} center vs. a square planar Pd^{II} center [59,61], the presence of *t*-butyl substituents and the rigidity of the macrocyclic ligand cannot accommodate a symmetric octahedral geometry preferred by a Pd^{IV} d^6 center [11,89]. For example, while [(N4)Pd^{III}MeCl]⁺ can be electrochemically oxidized at low temperature to generate an EPR silent red species that is likely a Pd^{IV} intermediate, this species cleanly converts back to the Pd^{III} complex within 1 h at RT. Moreover, a rapid comproportionation occurs when a solution of [(N4)Pd^{IV}MeCl]²⁺ is mixed with an equivalent amount of (N4)Pd^{II}MeCl to give [(N4)Pd^{III}MeCl]⁺ quantitatively (Scheme 5), supporting our hypothesis that the N4 ligand stabilizes preferentially the Pd^{III} oxidation state [118].

While these organometallic (N4)Pd^{III} complexes are stable in the dark, exposure to visible light leads to elimination of the homocoupled products ethane or biphenyl, the observed formation of ethane from monomethyl Pd complexes being unprecedented (Scheme 4, top). Moreover, the dimethyl complex (N4)Pd^{II}Me₂ has such a low Pd^{II}/Pd^{III} oxidation potential that it exhibits unprecedented oxidation reactivity and can react with mild oxidants such as O₂ or peroxides to generate the green species [(N4)Pd^{III}Me₂]⁺ that slowly reacts in absence of light to yield ethane and the monomethyl complex (N4)Pd^{II}Me(OH) (Scheme 4, bottom) [43].

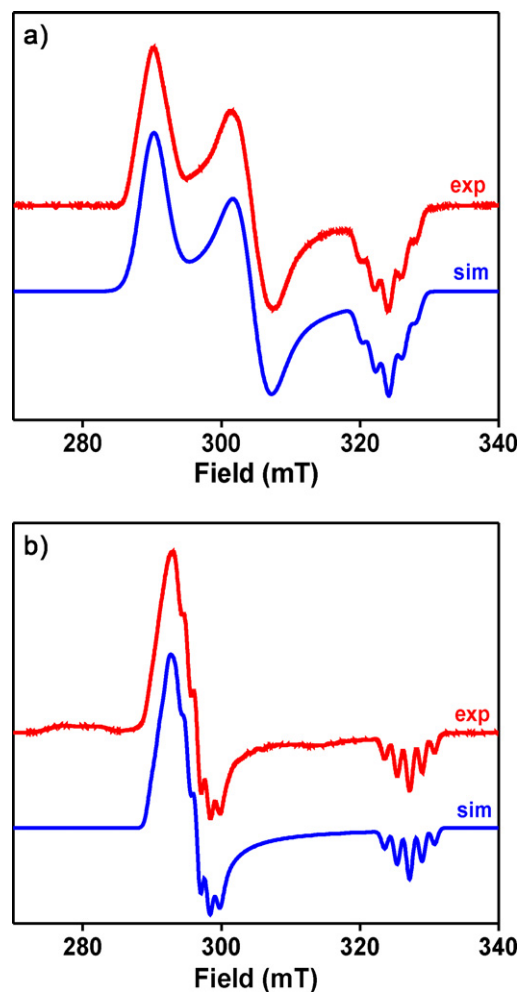


Fig. 5. Representative EPR Spectra of (N4)Pd^{III} complexes (1:3 MeCN:PrCN, 77 K). Simulation parameters: (a) [(N4)Pd^{III}MeCl]⁺, $g_x = 2.239$, $g_y = 2.134$, $g_z = 2.005$ ($A_z^{\text{N}} = 19$ G) [118]; (b) [(N4)Pd^{III}Me₂]⁺, $g_x = 2.221$ ($A_x^{\text{N}} = 12$ G), $g_y = 2.191$ ($A_y^{\text{N}} = 14$ G), $g_z = 1.986$ ($A_z^{\text{N}} = 18$ G) [43].

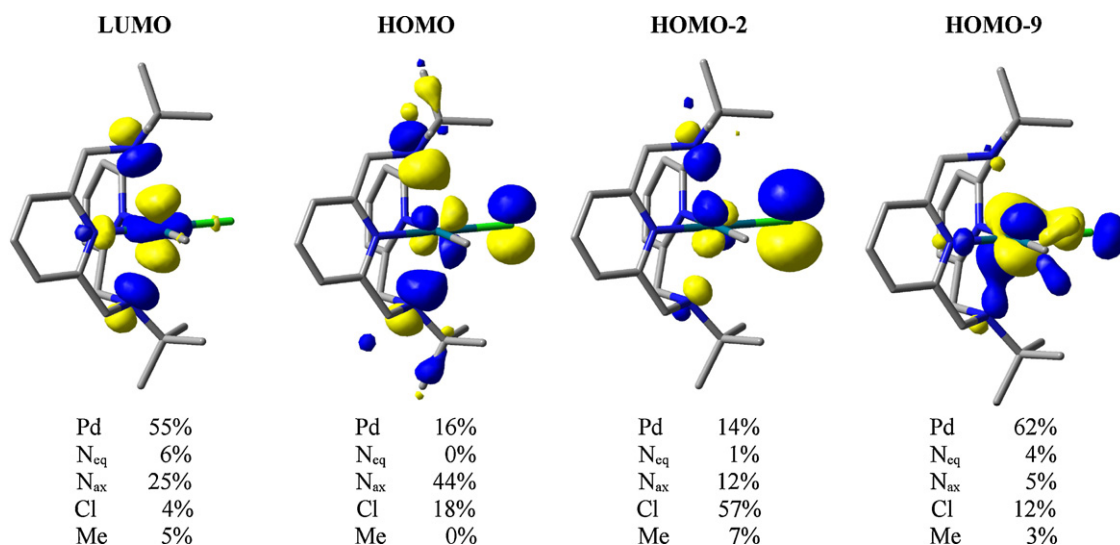


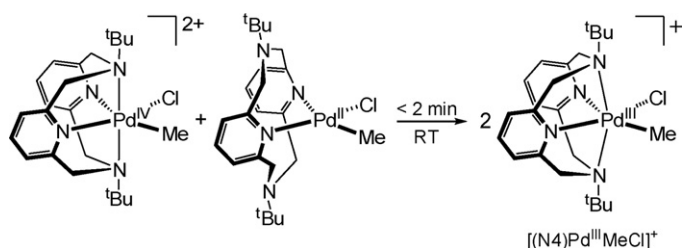
Fig. 6. DFT-calculated (UB3LYP/CEP-31G) β -MOs of [(N4)Pd^{III}MeCl]⁺ proposed to be involved in the observed UV–vis absorption bands (the calculated atomic contributions are listed for each MO) [118].

Table 2

TD-DFT calculated absorption bands $[(N4)Pd^{III}MeCl]^+$ and their composition and tentative assignment ($d-d$ or LMCT). Only the transitions with oscillator strengths greater than 0.006 are shown; the major contributing transitions have more than 6% contribution to the absorption band.

Wavelength (nm)	Oscillator strength	Major contributing transitions
720.7	0.034	HOMO(β) \rightarrow LUMO(β) (79%, LMCT)
539.2	0.007	HOMO-2(β) \rightarrow LUMO(β) (42%, LMCT) HOMO-9(β) \rightarrow LUMO(β) (22%, $d-d$)
404.1	0.082	HOMO-9(β) \rightarrow LUMO(β) (31%, $d-d$) HOMO-2(β) \rightarrow LUMO(β) (21%, LMCT) HOMO(β) \rightarrow LUMO(β) (9%, LMCT)
361.2	0.007	HOMO-3(β) \rightarrow LUMO(β) (24%, LMCT)
344.4	0.010	HOMO-5(β) \rightarrow LUMO(β) (31%, LMCT) HOMO-1(α) \rightarrow LUMO(α) (19%, LMCT)
324.0	0.036	HOMO(β) \rightarrow LUMO + 1(β) (13%, LMCT) HOMO-8(β) \rightarrow LUMO(β) (62%, LMCT)

A more detailed evaluation of the electronic properties of the $(N4)Pd^{III}$ complexes can provide insight into their spectroscopy and observed reactivity. The density functional theory (DFT) calculated frontier molecular orbitals and spin density distribution of the Pd^{III} complexes support the localization of the unpaired electron mainly on the Pd-based d_{z^2} atomic orbital (Fig. 6, LUMO). In addition, the UV–vis spectra of the $(N4)Pd^{III}$ complexes in MeCN show at least three absorption bands at 723–741, 554–594, and 353–386 nm (Fig. 7) [42]. Time dependent DFT (TD-DFT) calculations suggest that these bands can be assigned to LMCT transitions, a combination of $d-d$ and LMCT transitions, and LMCT transitions, respectively (Table 2 and Fig. 6). Interestingly, an appreciable overlap between the Pd orbitals and the amine N orbitals support a significant bonding interaction in the axial direction. Due to the rich absorption spectra of these organometallic Pd^{III} complexes, their observed photoreactivity could be due to either homolytic cleavage of the Pd–C bond or the dissociation of the axial ligand(s), however more detailed photochemical studies are needed to better understand their reactivity.



Scheme 5. Comproportionation of $[(N4)Pd^{IV}MeCl]^{2+}$ and $(N4)Pd^{II}MeCl$ complexes [118].

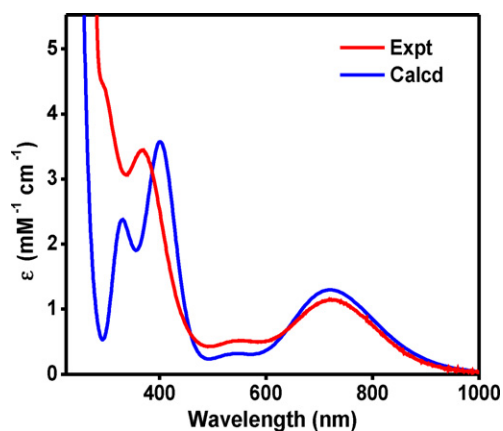


Fig. 7. UV–vis spectra of $[(N4)Pd^{III}MeCl]^+$: experimental spectrum in MeCN (red) and TD-DFT calculated (UB3LYP/CEP-31G/PCM) spectrum (blue) [118].

3. Dinuclear Pd(III) complexes

When two square planar Pd^{II} d^8 centers with an idealized D_{4h} symmetry are interacting along the z axis, a generalized molecular orbital diagram can be constructed in which both bonding and antibonding molecular orbitals are filled, resulting in a metal–metal bond order of zero (Fig. 8, left). When such dinuclear Pd^{II} complexes are oxidized by one or two electrons, removal of antibonding electrons is expected to lead to metal–metal bond orders of 0.5 and 1, respectively (Fig. 8, center and right).

3.1. Dinuclear Pd(II) precursors

Based on the above molecular orbital description, no bonding interaction between the two Pd^{II} centers is expected in dinuclear Pd^{II} complexes held together by bridging ligands [90]. However, a few Pd^{II} dinuclear species with metal–metal interactions have been described to date [91–98]. In these cases, the weak d^8-d^8 bonding interactions have been explained by the symmetry allowed mixing of the Pd $5p_z$ and $5s$ orbitals into the $4d_{z^2}$ orbitals of the Pd center [99–102], and DFT analyses have revealed calculated Pd–Pd bond orders of 0.10–0.15 [95,97].

We have recently reported Pd^{II} complexes supported by the macrocyclic tetradentate ligand 2,11-dithia[3.3](2,6)pyridinophane that display unique d^8-d^8 interactions between dicationic metal fragments and are not supported by any bridging ligands, strongly suggesting the existence of a significant metal–metal bonding character [98]. These d^8-d^8 bonding interactions are likely further enhanced by the presence of more covalent metal–S interactions and the overlap of the Pd $5d_{z^2}$ orbital with the axial pyridine ligand [98].

3.2. Mixed-valent Pd^{II}/Pd^{III} complexes

Oxidation by one electron of dinuclear Pd^{II} complexes is expected to increase metal–metal bonding character due to a Pd–Pd bond order of 0.5 (Fig. 8). Initial attempts to oxidize dinuclear Pd^{II} complexes have focused on a system employing di-*p*-tolylformamidinate ligands (Scheme 6) [90,103]. The corresponding one-electron oxidized product, $[Pd_2(DTolF)_4]PF_6$, was structurally characterized (Fig. 9a) and shown to exhibit a broad isotropic EPR signal ($g_{ave} = 2.014$), which was interpreted as arising from ligand-centered oxidation. By contrast, a similar dinuclear complex employing N,N' -diphenylbenzamidinate ligands, $[Pd_2(dpb)_4]ClO_4$, shows a well-defined axial EPR signal ($g_{||} = 1.98$, $g_{\perp} = 2.17$) with hyperfine coupling to ^{105}Pd in both directions, suggestive of a metal-centered oxidation (Scheme 6, Table 3) [104]. In addition, detailed electrochemical studies suggest that the forced proximity of two Pd^{II} centers along the z axis due to the four bridging ligands leads to a raising of the energy of the metal-centered

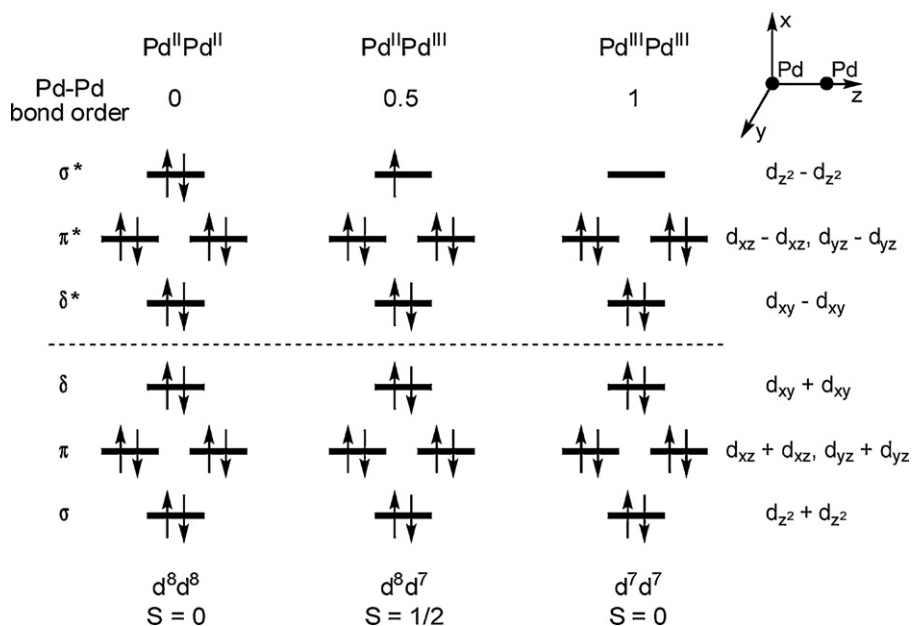


Fig. 8. Molecular orbital diagram for $\text{Pd}^{\text{II}}\text{Pd}^{\text{II}}$, $\text{Pd}^{\text{II}}\text{Pd}^{\text{III}}$, and $\text{Pd}^{\text{III}}\text{Pd}^{\text{III}}$ dinuclear complexes with interacting metal centers.

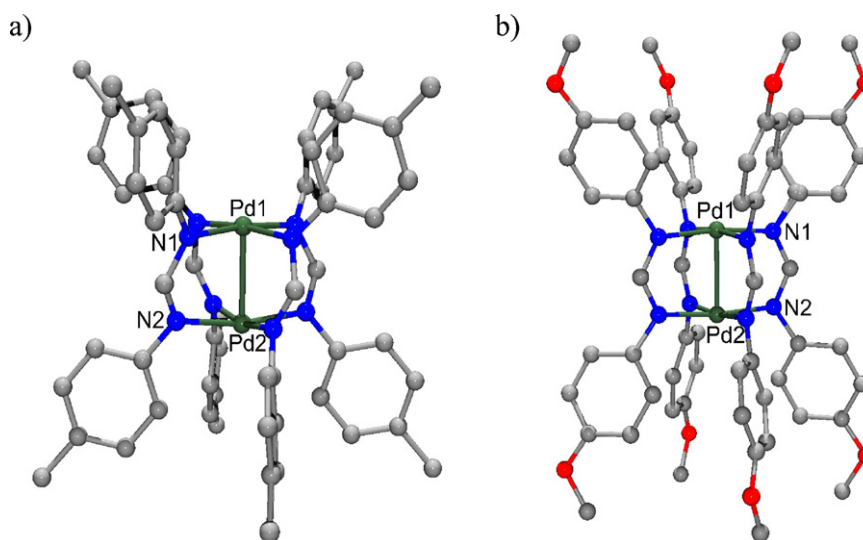
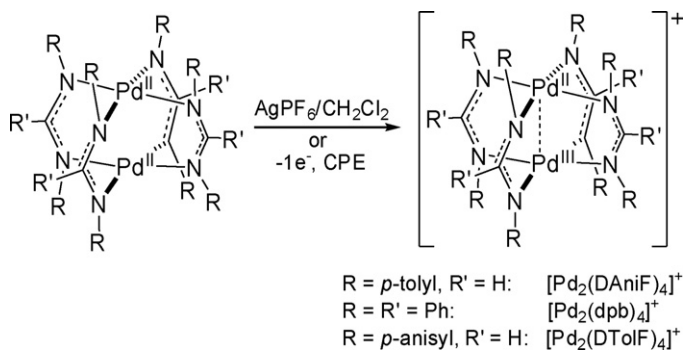


Fig. 9. Crystal structures of dinuclear $\text{Pd}^{\text{II}}\text{Pd}^{\text{III}}$ complexes. Selected bond distances (Å): (a) $[\text{Pd}_2(\text{DTolF})_4]^+$, Pd1–N1 2.03, Pd2–N2 2.05, Pd1–Pd2 2.635 [90]; (b) $[\text{Pd}_2(\text{DAniF})_4]^+$, Pd1–N1 2.044, Pd2–N2 2.036, Pd1–Pd2 2.597 [105]. Counteranions are omitted for clarity.



Scheme 6. Synthesis of formamidinate and benzamidinate dinuclear Pd^{III} complexes [90,103–105].

HOMO and a more facile one electron oxidation to generate the mixed-valent $\text{Pd}^{\text{II}}\text{Pd}^{\text{III}}$ species.

Another structurally characterized mixed-valent $\text{Pd}^{\text{II}}\text{Pd}^{\text{III}}$ complex dinuclear containing di-*p*-anisylformamidinate ligands, $[\text{Pd}_2(\text{DAniF})_4]\text{PF}_6$, was reported in 2007 [105]. This dark colored complex was obtained by one-electron oxidation of the $\text{Pd}^{\text{II}}\text{Pd}^{\text{II}}$ precursor and exhibits a Pd–Pd distance of 2.597 Å that is 0.052 Å shorter than that of the $\text{Pd}^{\text{II}}\text{Pd}^{\text{II}}$ analog, suggestive of an increase in the Pd–Pd bond order of 0.5 (Fig. 9b). While the X-band EPR spectrum of this mixed-valent $\text{Pd}^{\text{II}}\text{Pd}^{\text{III}}$ complex shows a broad isotropic signal, detailed EPR studies at high fields reveal a rhombic signal with a large spread of the *g* values (~ 0.03), suggesting that the unpaired electron resides mainly in metal-based molecular orbitals. In addition, the di-*p*-tolylformamidinate complex, which was previously characterized as a ligand-oxidized species due to an isotropic X-band EPR spectrum [90,103], exhibits anisotropic EPR

Table 3
Spectroscopic and electrochemical properties of dinuclear Pd^{II}Pd^{III} and Pd^{III}Pd^{III} complexes.

Complex	UV–vis, λ , nm (ϵ , M ⁻¹ cm ⁻¹)	Redox Potentials (vs. Fc/Fc ⁺) ^a	EPR, g_x, g_y, g_z (A values, G)	References
[Pd ₂ (DTolF) ₄]PF ₆	~860 (4500), ~680 (3000), 460 (4500) ^b	$E'_{1/2} = +0.32$ V $E''_{1/2} = +0.70$ V ^c	$g_{\perp} = 2.0259$, $g_{\parallel} = 1.9887$ ^d	[90,105]
[Pd ₂ (dph) ₄]ClO ₄	ND	$E_{1/2}^{II-III} = +0.17$ V ^e	$g_{\perp} = 2.17$ ($A_{\perp}^{Pd} = 33$ G), $g_{\parallel} = 1.99$ ($A_{\parallel}^{Pd} = 42$ G) ^{e,f}	[104]
[Pd ₂ (DAniF) ₄]PF ₆	~930 (1250), ~410 (950) ^b	$E'_{1/2} = +0.254$ V $E''_{1/2} = +0.506$ V $E'''_{1/2} = +0.674$ V $E^{IV} = +0.824$ V ^c	$g_x = 2.0286$, $g_y = 2.0136$, $g_z = 2.0004$ ^d	[105]
Pd ₂ (hpp) ₄ Cl ₂	648 (108), 324 (3300) ^b	$E_{1/2}^{II-III} = -0.304$ V $E_{pa}^{II-III/III-III} = +0.203$ V $E_{pa}^{III/III-III} = +0.203$ V ^c	NA	[106,107]
Pd ₂ (C ₆ H ₄ PPh ₂) ₂ (OAc) ₂ Cl ₂	499 (8700), 434 (1800), 379 (12,000) ^b	ND	NA	[108]
Pd ₂ (bqn) ₂ (OAc) ₂ Cl ₂	582 (2990), 491 (7390), 417 (26,100), 270 (36,900) ^b	$E_{1/2}^{II-III} = +0.42$ V ($\Delta E_p = 79$ mV), $E_{1/2}^{III-III} = +0.72$ V ($\Delta E_p = 114$ mV) ^c	NA	[35]
Pd ₂ (bqn) ₂ (OAc) ₄	419 (10,300), 281 (24,800) ^b	ND	NA	[36]
Pd ₂ (phpy) ₂ (OAc) ₄	436 (12,300), 316 (10,600) ^b	ND	NA	[36]
[(Me ₃ tacn) ₂ Pd ₂ Cl ₅]PF ₆	534 (21,000), 449 (sh, 4900), 360 (6100), 260 (43,000) ^g	$E_{1/2}^{II/III} = +0.055$ V, $E_{1/2}^{III/IV} = +0.163$ V ^h	ND ⁱ	[46]
[(Me ₃ tacn) ₂ Pd ₂ Br ₅]PF ₆	570 (25,000), 411 (8900), 273 (47 000) ^g	$E_{1/2}^{II/III} = +0.045$ V, $E_{1/2}^{III/IV} = +0.171$ V ^h	ND ⁱ	[46]
[(Me ₃ tacn) ₂ Pd ₂ Cl ₄ Br]PF ₆	546 (17,000), 378 (6800), 262 (41,000) ^g	$E_{1/2}^{II/III} = +0.065$ V, $E_{1/2}^{III/IV} = +0.174$ V ^h	ND ⁱ	[46]
[Pd ^{III} (bqn)(OAc)] _n F _n	1021 ^j , 464 ^k , 376 (2470) ^b	ND	NA	[112]
[Pd ^{2.5} (bqn)OAc] _n F _{0.5n}	991 ^j , 374 (2290) 345 (2270) ^b	ND	ND	[112]
(PPFI) ₂ Pd ₂ (X) ₄ (X = CF ₃ CO ₂ ⁻ or NO ₃ ⁻)	ND	ND	$g_{\parallel} = 3.200$ – 3.203 , $g_{\perp} = 1.908$ – 1.915 ^k	[40]
[(PPFI) ₂ Pd ₂ (μ -Cl) ₂]X ₂ (X = BF ₄ ⁻ or PF ₆ ⁻)	~380 (25,000), 915 (~2000)	$E_{1/2}^{II-III} = +0.11$ V $E_{pa}^{II-III/III-III} = +0.23$ V ^c	ND	[40]

ND: not determined; NA: not applicable.

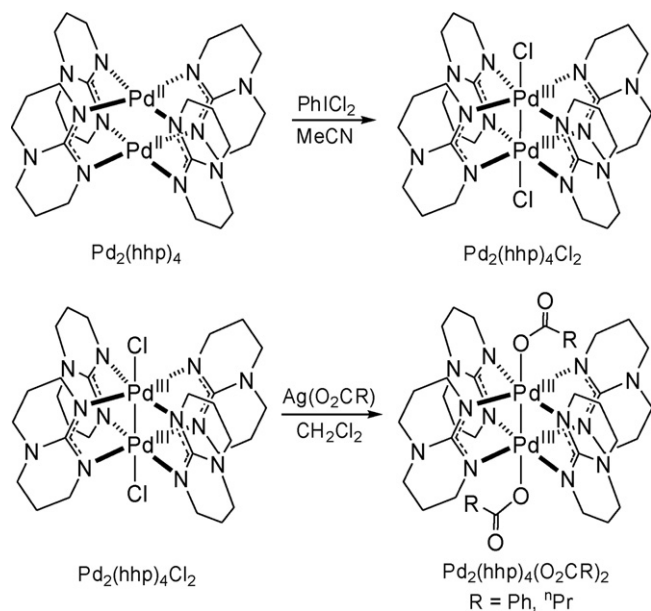
^a Determined for solutions of corresponding dinuclear Pd^{II} complexes.^b In CH₂Cl₂.^c In ⁿBu₄NPF₆/CH₂Cl₂.^d D-band (219.2 GHz), 4 K.^e In ⁿBu₄NClO₄/CH₂Cl₂.^f 123 K.^g In MeCN.^h In ⁿBu₄NPF₆/MeCN.ⁱ The two Pd^{III} centers are strongly antiferromagnetically coupled.^j The absorbance at this wavelength is non-linear with concentration.^k 110 K.spectra at high fields with a similarly large spread of the g values, in line with a metal-based unpaired electron (Table 3) [105].

3.3. Dinuclear Pd(III) complexes with a Pd–Pd bond

Dinuclear Pd^{III} complexes with a Pd–Pd interaction are expected to exhibit a metal–metal bond order of 1 (Fig. 8, right). The first such complex was synthesized in 1998 through the two-electron chemical oxidation by PhICl₂ of a paddlewheel dinuclear Pd^{II} complex containing the 1,3,4,6,7,8-hexahydro-2H-pyrimido[1,2-a]pyrimidine (hpp) ligand (Scheme 7, top) [106]. The resulting dinuclear Pd^{III} complex Pd₂(hpp)₄Cl₂ exhibits metal centers with distorted octahedral geometries and the shortest Pd–Pd bond ever reported (2.391 Å), 0.164 Å shorter than the Pd–Pd distance in the Pd^{II} precursor (Fig. 10). This decrease in the metal–metal distance suggests that the oxidation occurs at the Pd centers and leads to a significant metal–metal bonding interaction, which was confirmed by the calculated $d_{z^2-d_{z^2}}$ σ bonding character of the HOMO [106]. The same ligand was employed recently to yield a dinuclear Pd^{III} complex in which the axial Cl⁻ ligands were substituted with carboxylate ions in presence of Ag⁺ salts (Scheme 7, bottom) [107].

The first organometallic dinuclear Pd^{III} complexes were reported in 2006 by Cotton et al. (Scheme 8, top) [108]. The Pd^{III} centers are held together by two orthometalated phosphine ligands and two carboxylate groups, one chloride anion being bound to each metal center *trans* to the Pd–Pd bond (Fig. 11). The observed short Pd–Pd distances of 2.524–2.543 Å and DFT calculations support the presence of a single bond between the two Pd centers, while the axial chloride ligands seem to lead to a lengthening of the metal–metal bond [108]. Similar organometallic dinuclear Pd^{III} complexes have been recently reported in diborylation reaction studies [109,110]. In addition, the presence of a square planar Pd center in a formal +3 oxidation state has been proposed recently in a heterobimetallic phosphido-bridged Pd–Pt complex [111].

Organometallic dinuclear Pd^{III} complexes have been shown recently to be catalytically active intermediates in oxidative C–heteroatom bond formation reactions [35–38]. For example, a cyclopalladated benzo[h]quinolonyl (bqn) dinuclear Pd^{II} complex bridged by two acetate groups can be oxidized by PhICl₂ to generate a dark red-brown dinuclear Pd^{III} species Pd₂(bqn)₂(OAc)₂Cl₂ ($\lambda_{\max} = 417$ nm, Table 3; Scheme 8, middle). The complex is diamagnetic and exhibits a Pd–Pd distance of 2.567 Å, suggesting the presence of a Pd–Pd single bond (Fig. 12a) [35]. Another dinuclear



Scheme 7. Synthesis of $\text{Pd}_2(\text{hpp})_4\text{X}_2$ complexes [106,107].

Pd^{III} complex, $\text{Pd}_2(\text{phpy})_2(\text{OAc})_4$, with a similar Pd–Pd distance (2.555 Å) was later obtained by oxidation of a 2-phenylpyridyl (phpy) Pd^{II} diacetate dimer with $\text{PhI}(\text{OAc})_2$ (Scheme 8, bottom; Fig. 12b) [36]. While these organometallic dinuclear Pd^{III} are stable at low temperatures, they undergo reductive elimination upon warming to room temperature and lead to C–heteroatom bond formation. Detailed mechanistic studies suggest a synergistic involvement of the two Pd centers during both oxidation and reductive elimination [35,36,38]. Several recent reviews have described in detail the involvement of dinuclear Pd^{III} complexes as active intermediates in catalytic oxidative C–H functionalization reactions and will not be discussed herein [23,39].

Interestingly, the oxidation of the benzo[h]quinoliny dinuclear Pd^{II} complex with 1 equiv XeF_2 in absence of coordinating anions leads to the synthesis of 1D molecular wires containing Pd^{III} centers (Scheme 9, top) [112]. The X-ray structure of the oxidized dark-red product exhibits an infinite chain of

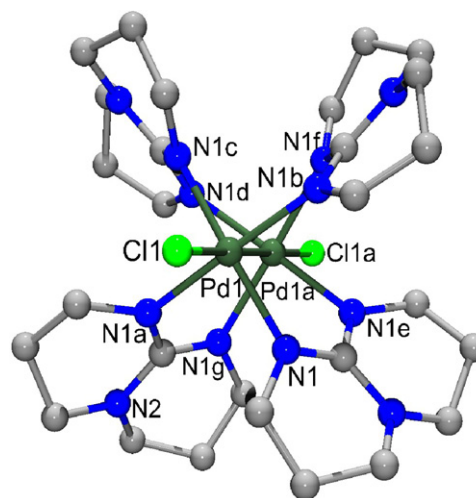


Fig. 10. Structure of the first dinuclear Pd^{III} complex, $\text{Pd}_2^{\text{III}}(\text{hpp})_4\text{Cl}_2$ [106]. Selected bond distances (Å): Pd1–N1 2.034, Pd1–Cl1 2.474, Pd1–Pd1a 2.391 (all Pd–N bond lengths are identical due to symmetry).

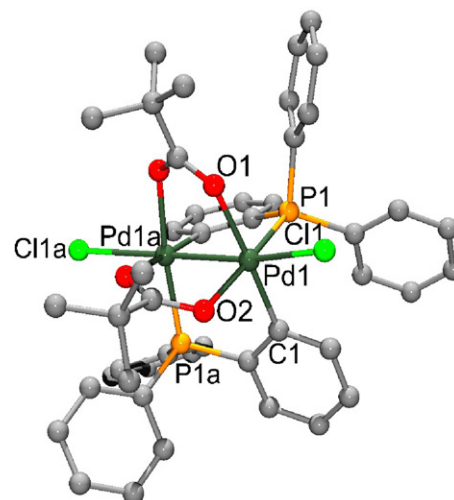


Fig. 11. Structure of organometallic Pd^{III} dinuclear complex $\text{Pd}_2^{\text{III}}(\text{C}_6\text{H}_4\text{PPh}_2)_2(\text{OAc})_2\text{Cl}_2$ [108]. Selected bond distances (Å): Pd1–Cl1 2.426, Pd1–P1 2.262, Pd1–C1 2.029, Pd1–O1 2.134, Pd1–O2 2.103, Pd1–Pd1a 2.524.

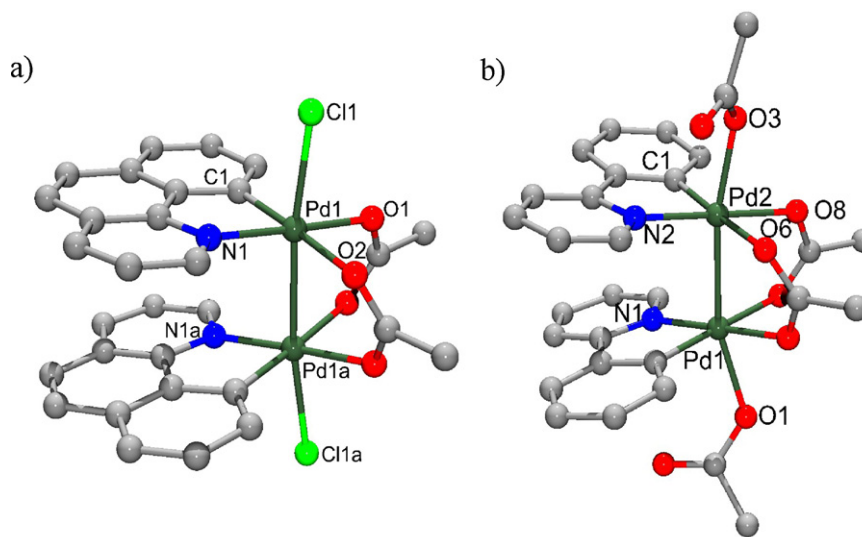


Fig. 12. X-ray structures of dinuclear Pd^{III} palladacycle complexes. Selected bond distances (Å): (a) $(\text{bqn})_2\text{Pd}_2^{\text{III}}(\text{OAc})_2\text{Cl}_2$, Pd1–N1 2.017, Pd1–C1 1.999, Pd1–O1 2.042, Pd1–O2 2.133, Pd1–Cl1 2.417, Pd1–Pd1a 2.567 [35]; (b) $(\text{phpy})_2\text{Pd}_2^{\text{III}}(\text{OAc})_4$, Pd2–N2 2.002, Pd2–C1 1.280, Pd2–O6 2.139, Pd2–O8 2.061, Pd2–O3 2.130, Pd2–Pd1 2.555 [36]. Solvent molecules are omitted for clarity.

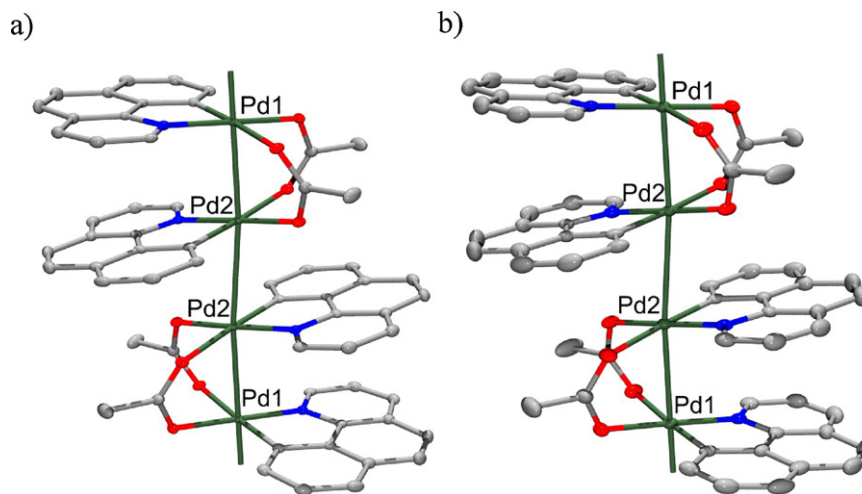
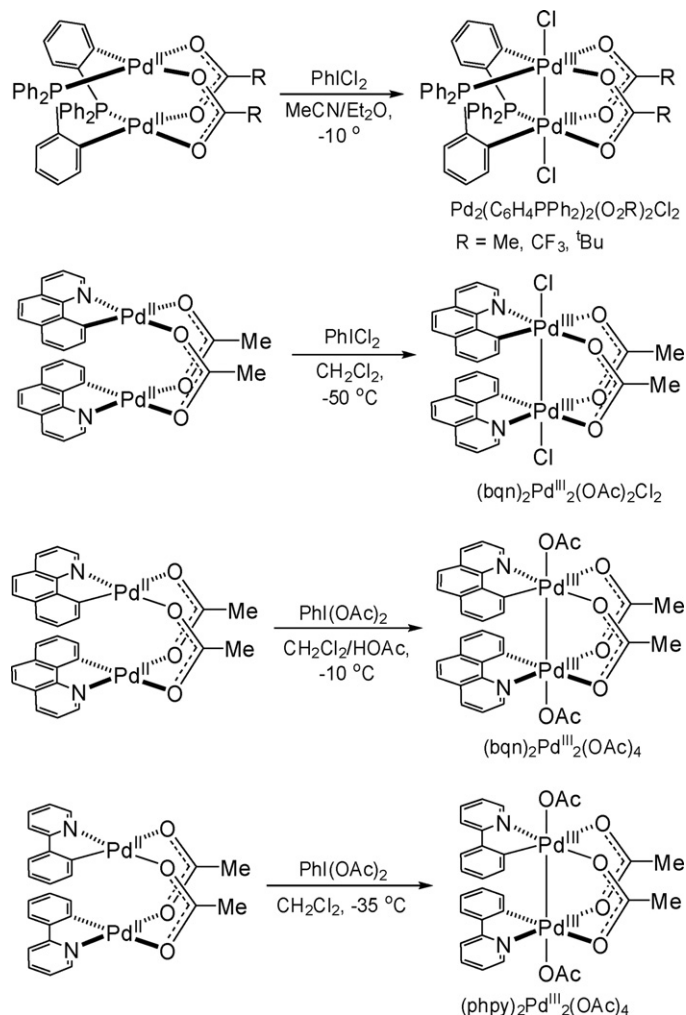


Fig. 13. Structures of fragments from 1D chains containing Pd–Pd interactions [112]. Selected bond distances (Å): (a) [(bqn)Pd^{III}(OAc)]_n(F)_n, Pd1–Pd2 2.721; Pd1–Pd1 2.972, Pd2–Pd2 2.982; (b) [(bqn)Pd^{2.5}(OAc)]_nF_{0.5n}, Pd1–Pd2 2.727; Pd1–Pd1 2.980, Pd2–Pd2 2.980. Counteranions and solvent molecules are omitted for clarity.

Pd^{III} cations and non-coordinated fluoride anions, with acetate-bridged Pd–Pd distances of 2.72 Å and unsupported interdimer Pd–Pd distances of 2.98 Å (Fig. 13a). The persistence of the extended 1D chain structure in solution was confirmed by dynamic and static light scattering measurements and the presence of a

concentration-dependent NIR absorption [112]; however, addition of chloride leads to quantitative formation of dinuclear Pd^{III} species (Scheme 9, top). Oxidation of the Pd^{II} precursor with 0.5 equiv of XeF₂ leads to formation of an extended 1D chain with an average oxidation state of Pd^{2.5} (Scheme 9, bottom; Fig. 13b). The molecular wires based on Pd^{III} centers exhibit semiconductor properties with an adjustable bandgap (depending on counterion and bridging carboxylate), while the Pd^{2.5} wires display metallic conductivity above 200 K; such a metallic state has not been reported previously for any molecular 1D wires [112].



Scheme 8. Synthesis of dinuclear Pd^{III} palladacycle complexes [35,36,108].

3.4. Dinuclear Pd(III) complexes without a Pd–Pd bond

A series of dinuclear Pd^{III} complexes supported by the common tridentate nitrogen-donor ligand *N,N,N'*-trimethyl-1,4,7-triazacyclononane (Me₃tacn) were reported by our group in 2011; these complexes are the first dinuclear Pd^{III} complexes that are not stabilized by a Pd–Pd bond [46]. CV studies of the Pd^{II} precursors (Me₃tacn)Pd^{II}X₂ (X: Cl, Br) reveal two closely spaced oxidation waves at low potentials (Fig. 14, Table 3). Electrochemical

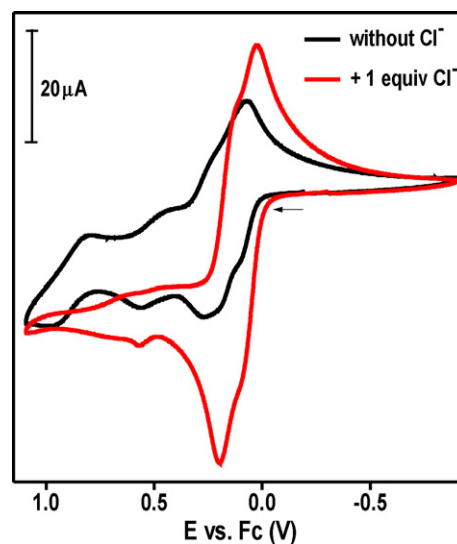
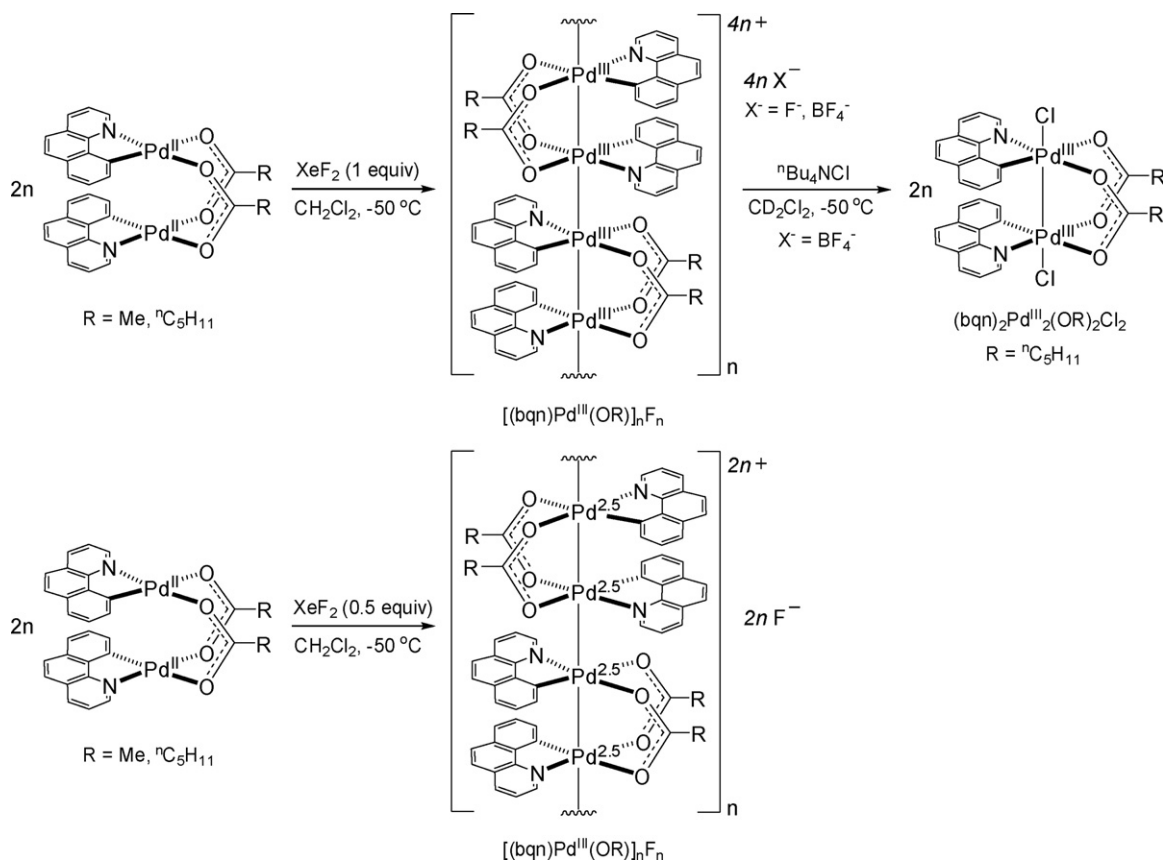
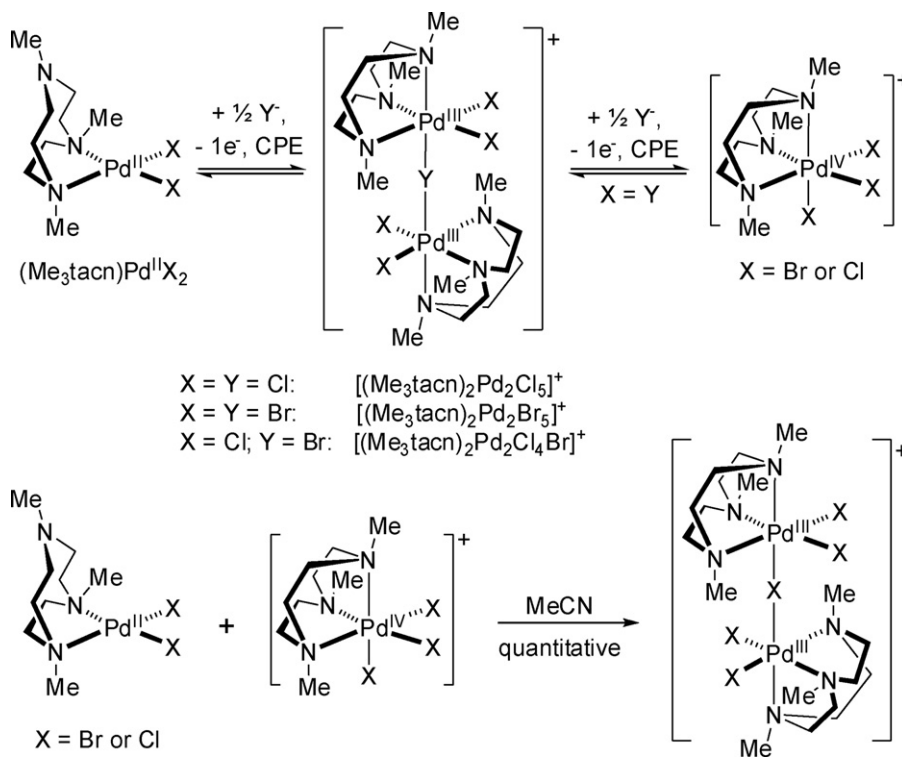


Fig. 14. Cyclic voltammograms of (Me₃tacn)PdCl₂ in absence (black line) and presence (red line) of 1 equiv Cl⁻ (5 mM in 0.1 M Bu₄NPF₆/MeCN, 100 mV/s scan rate) [46].



Scheme 9. Synthesis of one-dimensional Pd^{III} palladacycle wires [112].



Scheme 10. Synthesis of $[(\text{Me}_3\text{tacn})_2\text{Pd}_2\text{X}_4(\mu\text{-Y})](\text{PF}_6)$ complexes ($\text{X}, \text{Y} = \text{Cl}, \text{Br}$) [46].

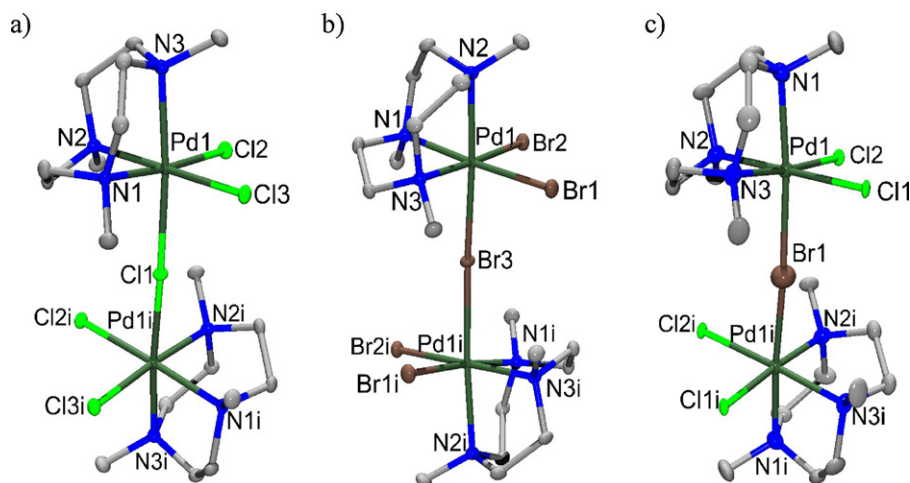


Fig. 15. Crystal structures of dinuclear $(\text{Me}_3\text{tacn})\text{Pd}^{\text{III}}$ complexes [46]. Selected bond distances (Å) and angles ($^\circ$): (a) $[(\text{Me}_3\text{tacn})_2\text{Pd}_2\text{Cl}_5]^+$, Pd1–N1 2.094, Pd1–N2 2.105, Pd1–N3 2.273, Pd1–Cl2 2.3179, Pd1–Cl3 2.322, Pd1–Cl1 2.480, Cl1–Pd1i 2.480, Pd1–Pd1i 4.931, Pd1–Cl1–Pd1i 167.5; (b) $[(\text{Me}_3\text{tacn})_2\text{Pd}_2\text{Br}_5]^+$, Pd1–N1 2.104, Pd1–N3 2.120, Pd1–N2 2.286, Pd1–Br1 2.432, Pd1–Br2 2.437, Pd1–Br3 2.587, Br3–Pd1i 2.587, Pd1–Pd1i 5.133, Pd1–Br3–Pd1i 165.4; (c) $[(\text{Me}_3\text{tacn})_2\text{Pd}_2\text{Cl}_4\text{Br}]^+$, Pd1–N3 2.082, Pd1–N2 2.093, Pd1–N1 2.273, Pd1–Cl2 2.350, Pd1–Cl1 2.363, Pd1–Br1 2.539, Pd1–Pd1i 5.031, Pd1–Br1–Pd1i 164.3. Counteranions and solvent molecules are omitted for clarity.

oxidation of these Pd^{II} complexes by one electron leads to formation of dark-purple species whose X-ray structures reveal dinuclear cations $[(\text{Me}_3\text{tacn})\text{Pd}^{\text{III}}\text{X}_2(\mu\text{-X})\text{Pd}^{\text{III}}\text{X}_2(\text{Me}_3\text{tacn})]^+$ (X: Cl, X: Br) in which a single halide ion bridges the two Pd^{III} centers (Scheme 10). Each metal center has a distorted octahedral geometry with two N atoms and the two terminal halides in the equatorial plane, while the third N atom of Me_3tacn and the bridging halide occupy the axial positions (Fig. 15). Interestingly, addition of 0.5 equiv of external halide during electrolysis leads to formation of the dinuclear Pd^{III} complexes in high yield, and also provides a synthetic method to generate a mixed-halide complex (Fig. 15c and Scheme 10, top). The short Pd...Pd distances and the strong antiferromagnetic coupling between the unpaired d_{z^2} electrons of the two Pd^{III} centers suggest an intimate orbital overlap between Pd and the bridging halide in these complexes (vide infra). Moreover, these dinuclear Pd^{III} complexes also represent a model of the delocalized $\text{Pd}^{\text{III}}\text{-X-Pd}^{\text{III}}$ electronic structure that has been proposed to exist in some -Pd-X-Pd-X- one-dimensional (1D) chains [113,114].

Further electrochemical oxidation of the dinuclear Pd^{III} species in presence of 0.5 equiv halide generates mononuclear Pd^{IV} complexes (Scheme 10, top). Interestingly, a rapid comproportionation reaction occurs between 1 equiv of the mononuclear Pd^{II} complex and 1 equiv of the mononuclear Pd^{IV} species to generate the dinuclear Pd^{III} complex in quantitative yield (Scheme 10, bottom), suggesting that these dinuclear Pd^{III} complexes are more stable than the corresponding mononuclear Pd^{IV} and Pd^{II} complexes under an analogous ligand environment. The reversible interconversion of dinuclear Pd^{III} and mononuclear Pd^{IV} species parallels the proposed involvement of analogous intermediates in Pd-catalyzed C–H oxidative functionalization reactions and suggests that for a given ligand environment both types of intermediates can be present [35–37]. This study also provided evidence for the involvement of a Pd^{III} species in the Kharasch addition of polyhaloalkanes to alkenes and confirms the ability of Pd to catalyze one-electron radical reactions [46].

The above dinuclear Pd^{III} complexes exhibit unique electronic properties. Their UV–vis spectra in MeCN reveal at least three intense absorption bands at 535–570, 360–410, and 260–280 nm, respectively (Table 3 and Fig. 16). For all three complexes, the ~ 550 nm absorptions exhibit an uncommonly large extinction coefficients ($\epsilon > 17,000 \text{ L mol}^{-1} \text{ cm}^{-1}$, Fig. 16) and were assigned to an intermetallic Pd-to-Pd charge transfer (MMCT) transition [115] that is strongly mixed with a $\mu\text{-Cl}$ -to-Pd CT transition (LMCT)

[113,114]. TD-DFT calculations support such an assignment by revealing a large oscillator strength for the HOMO to LUMO + 1 transition, where the HOMO exhibits σ -bonding Pd– $\mu\text{-Cl}$ character and the LUMO + 1 has antibonding Pd– $\mu\text{-Cl}$ character (Fig. 17, Table 4). The higher energy absorption bands can be assigned to a combination of bridging and terminal halide-to-Pd LMCT bands (Fig. 17, Table 4) [113,114]. The replacement of Cl^- with Br^- ligands leads to lower energies of all transitions and thus supports the halide contributions to the corresponding MOs (Table 3, Fig. 17) [116].

Stabilization of the Pd^{III} state has been achieved recently in halogen-bridged -Pd-X-Pd-X- 1D chain compounds with N-donor ligands by using counteranions with long alkyl chains or in mixed Ni/Pd 1D chain compounds [113,114,117]. For example, the 1D chain compound $[\text{Pd}(\text{en})_2\text{Br}](\text{C}_5\text{-Y})$ (en: ethylenediamine; $\text{C}_5\text{-Y}$: dipentylsulfosuccinate) exists in an average-valent Pd^{III} state at a temperatures below 200 K, as confirmed by X-ray, EPR, and Raman spectroscopy studies (Scheme 11) [113,114].

Recently, the first examples of paramagnetic dinuclear Pd^{III} complexes have been reported [40]. These complexes were obtained by chemical or electrochemical oxidation of Cl-bridged pentaphenylferrocenyl imidazoline or oxazoline palladacycles (Scheme 12). The oxidation of the Pd^{II} centers instead of the

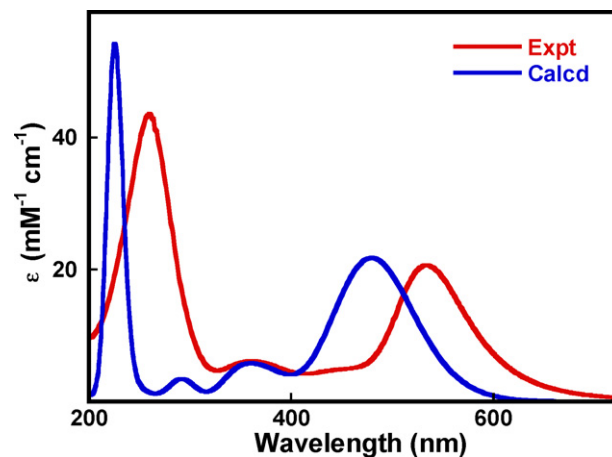


Fig. 16. UV–vis spectra of $[(\text{Me}_3\text{tacn})\text{Pd}^{\text{III}}\text{Cl}_2(\mu\text{-Cl})\text{Pd}^{\text{III}}\text{Cl}_2(\text{Me}_3\text{tacn})]^+$: experimental spectrum in MeCN (red) and normalized TD-DFT calculated (UB3LYP/CEP-31G/gas phase) spectrum (blue) [46].

Table 4
TD-DFT calculated absorption bands for $[(\text{Me}_3\text{tacn})\text{Pd}^{\text{III}}\text{Cl}_2(\mu\text{-Cl})\text{Pd}^{\text{III}}\text{Cl}_2(\text{Me}_3\text{tacn})]^{2+}$ and their composition and tentative assignment (MMCT or LMCT). Only the transitions with oscillator strengths greater than 0.05 are shown; the major contributing transitions have more than 6% contribution to the absorption band.

Wavelength (nm)	Oscillator strength	Major contributing transitions
488.8	0.350	HOMO \rightarrow LUMO + 1 (50%, MMCT) HOMO-1 \rightarrow LUMO + 1 (12%, LMCT)
451.4	0.168	HOMO \rightarrow LUMO + 1 (24%, MMCT) HOMO-9 \rightarrow LUMO + 1 (23%, LMCT)
377.8	0.057	HOMO-10 \rightarrow LUMO + 1 (24%, LMCT) HOMO-2 \rightarrow LUMO + 1 (19%, LMCT) HOMO-3 \rightarrow LUMO + 1 (15%, LMCT)
345.7	0.068	HOMO-8 \rightarrow LUMO + 1 (38%, LMCT) HOMO-10 \rightarrow LUMO + 1 (32%, LMCT)
291.8	0.085	HOMO-11 \rightarrow LUMO + 1 (84%, LMCT)
225.5	0.539	HOMO-15 \rightarrow LUMO (28%, LMCT)
225.2	0.717	HOMO-14 \rightarrow LUMO + 2 (24%, LMCT) HOMO-12 \rightarrow LUMO + 2 (24%, LMCT)

Fe^{II} centers has been proposed based on XAS, EPR, Mössbauer, and electrochemical studies. The acetate/hydroxo bridged complex $[(\text{PPFI})_2\text{Pd}_2(\mu\text{-OAc})(\mu\text{-OH})](\text{BF}_4)_2$ was characterized by X-ray crystallography (Fig. 18), which reveals the presence of square

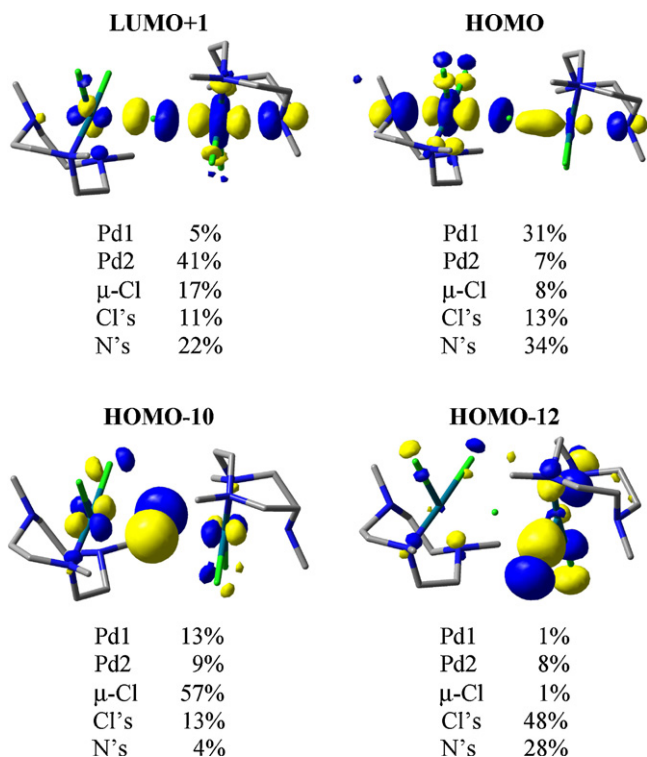
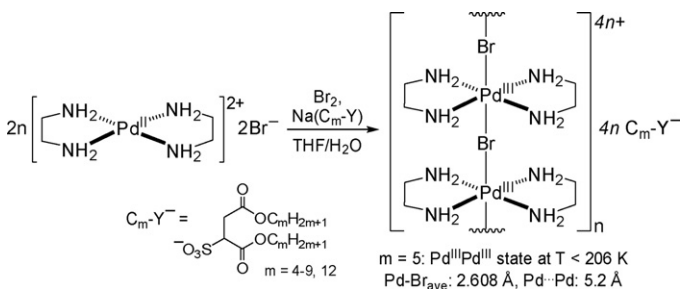
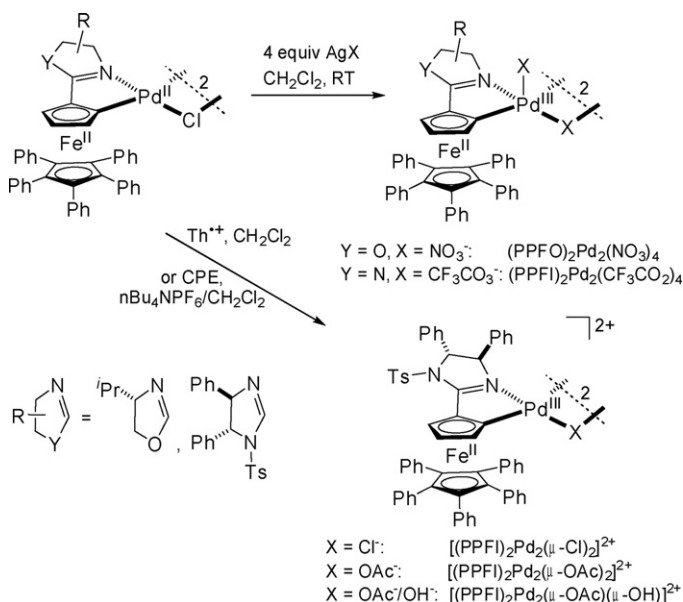


Fig. 17. DFT-calculated (UB3LYP/CEP-31G, broken symmetry) α -MOs of $[(\text{Me}_3\text{tacn})\text{Pd}^{\text{III}}\text{Cl}_2(\mu\text{-Cl})\text{Pd}^{\text{III}}\text{Cl}_2(\text{Me}_3\text{tacn})]^{2+}$ proposed to be involved in the observed UV–vis absorption bands (the calculated atomic contributions are listed for each MO) [46].



Scheme 11. Synthesis of quasi-one-dimensional halogen-bridged Pd complexes [113,114].



Scheme 12. Synthesis of pentaphenylferrocenyl imidazoline and oxazoline-derived dinuclear Pd^{III} complexes (Th^+ : thianthrenyl cation radical) [40].

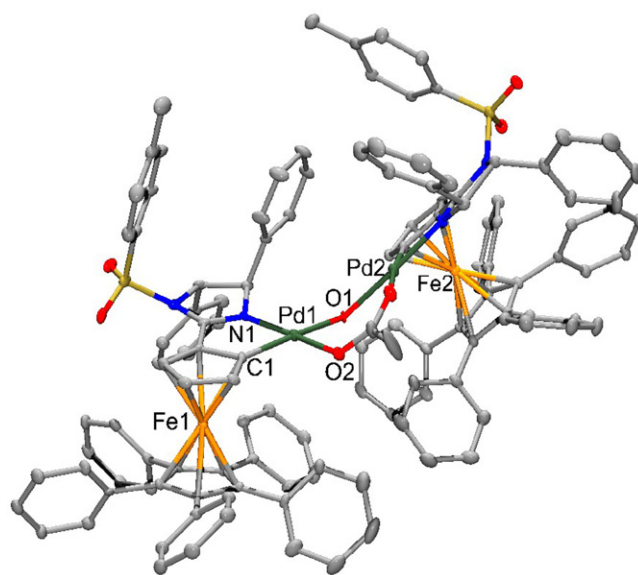


Fig. 18. Structure of $[(\text{PPFO})_2\text{Pd}^{\text{III}}_2(\mu\text{-OAc})(\mu\text{-OH})]^{2+}$ (PPFO: pentaphenylferrocenyl oxazoline) [40]. Selected bond distances (Å) and angles (°): Pd1-N1 1.999, Pd1-C1 1.966, Pd1-O1 2.166, Pd1-O2 2.006, $\text{Pd1} \cdots \text{Pd2}$ 3.574, Pd1-O1-Pd2 110.9.

planar Pd centers, while EXAFS analysis for the trifluoroacetate-bridged species $(\text{PPFI})_2\text{Pd}_2(\text{CF}_3\text{CO}_2)_4$ suggests the presence of five-coordinate Pd centers. These dinuclear Pd^{III} complexes are also active catalysts for asymmetric aza-Claisen rearrangements [40].

4. Summary and outlook

The isolation and characterization of compounds containing Pd^{III} centers has begun almost three decades ago. The first Pd^{III} ionic compound, NaPdF_4 , and several analogous compounds have been reported in the early 1980s. In addition, the first Werner-type coordination complexes containing Pd^{III} centers have been reported in the late 1980s, and during the same time the first mixed-valent $\text{Pd}^{\text{II}}\text{Pd}^{\text{III}}$ complexes were also characterized. By comparison, the first dinuclear Pd^{III} complex was reported in 1998, while the first organometallic dinuclear Pd^{III} complexes were reported in 2006 and their reductive elimination reactivity was described in 2009. It was not until 2010 that the first mononuclear organometallic complexes were reported and their reactivity investigated. In these systems, judiciously designed ligands have been extensively employed for the synthesis and stabilization of Pd^{III} species. In the past few years a large number of Pd^{III} intermediates have been isolated, characterized, and proposed to play a role in a range of one- and two-electron chemical transformations such as oxidative C–H functionalization reactions, C–C coupling reactions, and radical insertion and addition reactions. For all these systems, a detailed understanding of their steric and electronic properties is needed in order to design optimal ligand environments for the targeted chemical reactions. We envision that in the near future the chemistry of less-common odd-electron oxidation states of Pd, as well as other second and third row transition metals, will lead to novel redox reactions that resemble the reactivity profiles of first row transition metals, which typically display odd-electron oxidation states. Such new reactivity profiles are expected to find applications in various areas of chemistry, from organometallic catalysis to multi-electron redox transformations and small molecule activation relevant to renewable energy utilization.

Acknowledgments

We thank the Department of Chemistry at Washington University, the American Chemical Society Petroleum Research Fund (49914-DNI3), and DOE Catalysis Science Program (DE-FG02-11ER16254) for financial support. L.M.M. is a Sloan Fellow.

References

- [1] P.M. Henry, Palladium Catalyzed Oxidation of Hydrocarbons, D. Reidel, Boston, 1980.
- [2] E. Negishi, Handbook of Organopalladium Chemistry for Organic Synthesis, John Wiley & Sons, Hoboken, NJ, 2002.
- [3] J.F. Hartwig, Organotransition Metal Chemistry: From Bonding to Catalysis, University Science Books, Sausalito, 2010.
- [4] R.F. Service, Science 330 (2010) 308.
- [5] F.A. Cotton, G. Wilkinson, C.A. Murillo, M. Bochmann, Advanced Inorganic Chemistry, John Wiley & Sons, New York, 1999.
- [6] N. Miyaura, A. Suzuki, Chem. Rev. 95 (1995) 2457.
- [7] S.S. Stahl, Angew. Chem. Int. Ed. 43 (2004) 3400.
- [8] B.M. Stoltz, Chem. Lett. 33 (2004) 362.
- [9] K.M. Gligorich, M.S. Sigman, Chem. Commun. (2009) 3854.
- [10] P.K. Byers, A.J. Canty, B.W. Skelton, A.H. White, J. Chem. Soc., Chem. Commun. (1986) 1722.
- [11] A.J. Canty, Acc. Chem. Res. 25 (1992) 83.
- [12] P.L. Alsters, P.F. Engel, M.P. Hogerheide, M. Copijn, A.L. Spek, G. van Koten, Organometallics 12 (1993) 1831.
- [13] R. van Asselt, E. Rijnberg, C.J. Elsevier, Organometallics 13 (1994) 706.
- [14] R. van Belzen, H. Hoffmann, C.J. Elsevier, Angew. Chem. Int. Ed. 36 (1997) 1743.
- [15] M.-C. Lagunas, R.A. Gossage, A.L. Spek, G. van Koten, Organometallics 17 (1998) 731.
- [16] Y. Yamamoto, T. Ohno, K. Itoh, Angew. Chem. Int. Ed. 41 (2002) 3662.
- [17] Y. Yamamoto, S. Kuwabara, S. Matsuo, T. Ohno, H. Nishiyama, K. Itoh, Organometallics 23 (2004) 3898.
- [18] J. Campora, P. Palma, D. del Rio, E. Carmona, C. Graiff, A. Tiripicchio, Organometallics 22 (2003) 3345.
- [19] J. Campora, P. Palma, D. del Rio, J.A. Lopez, P. Valerga, Chem. Commun. (2004) 1490.
- [20] A.R. Dick, K.L. Hull, M.S. Sanford, J. Am. Chem. Soc. 126 (2004) 2300.
- [21] A.J. Canty, J. Chem. Soc., Dalton Trans. (2009) 10409.
- [22] K. Muniz, Angew. Chem. Int. Ed. 48 (2009) 9412.
- [23] T.W. Lyons, M.S. Sanford, Chem. Rev. 110 (2010) 1147.
- [24] P. Sehnal, R.J.K. Taylor, I.J.S. Fairlamb, Chem. Rev. 110 (2010) 824.
- [25] L.-M. Xu, B.-J. Li, Z. Yang, Z.-J. Shi, Chem. Soc. Rev. 39 (2010) 712.
- [26] Recent examples of isolated Pd^{IV} intermediates:
 - (a) A.R. Dick, J.W. Kampf, M.S. Sanford, J. Am. Chem. Soc. 127 (2005) 12790;
 - (b) S.R. Whitfield, M.S. Sanford, J. Am. Chem. Soc. 129 (2007) 15142;
 - (c) R.Y. Guo, J.L. Portscher, V.W. Day, H.C. Malinakova, Organometallics 26 (2007) 3874;
 - (d) T. Furuya, T. Ritter, J. Am. Chem. Soc. 130 (2008) 10060;
 - (e) N.D. Ball, M.S. Sanford, J. Am. Chem. Soc. 131 (2009) 3796;
 - (f) J.M. Racowski, A.R. Dick, M.S. Sanford, J. Am. Chem. Soc. 131 (2009) 10974;
 - (g) P.L. Arnold, M.S. Sanford, S.M. Pearson, J. Am. Chem. Soc. 131 (2009) 13912;
 - (h) N.D. Ball, J.W. Kampf, M.S. Sanford, J. Am. Chem. Soc. 132 (2010) 2878;
 - (i) W. Oloo, P.Y. Zavali, J. Zhang, E. Khaskin, A.N. Vedernikov, J. Am. Chem. Soc. 132 (2010) 14400;
 - (j) O. Daugulis, H.-Q. Do, D. Shabashov, Acc. Chem. Res. 42 (2009) 1074;
 - (k) D. Shabashov, O. Daugulis, J. Am. Chem. Soc. 132 (2010) 3965;
 - (l) H.C. Malinakova, Top. Organomet. Chem. 503 (2011) 85;
 - (m) A.S. McCall, H. Wang, J.M. Desper, S. Kraft, J. Am. Chem. Soc. 133 (2011) 1832.
- [27] R. Vilar, D.M.P. Mingos, C.J. Cardin, J. Chem. Soc., Dalton Trans. (1996) 4313.
- [28] V. Dura-Vila, D.M.P. Mingos, R. Vilar, A.J.P. White, D.J. Williams, Chem. Commun. (2000) 1525.
- [29] T. Murahashi, T. Otani, E. Mochizuki, Y. Kai, H. Kurosawa, S. Sakaki, J. Am. Chem. Soc. 120 (1998) 4536.
- [30] T. Murahashi, T. Nagai, T. Okuno, T. Matsutani, H. Kurosawa, Chem. Commun. (2000) 1689.
- [31] C.M. Fafard, D. Adhikari, B.M. Foxman, D.J. Mendiola, O.V. Ozerov, J. Am. Chem. Soc. 129 (2007) 10318.
- [32] R. Huacuja, D.J. Graham, C.M. Fafard, C.-H. Chen, B.M. Foxman, D.E. Herbert, G. Alliger, C.M. Thomas, O.V. Ozerov, J. Am. Chem. Soc. 133 (2011) 3820.
- [33] J. Zhang, R. Pattacini, P. Braunstein, Inorg. Chem. 48 (2009) 11954.
- [34] Formation of a few transient Pd^{I} species has been proposed based on EPR:
 - (a) K. Broadley, G.A. Lane, N.G. Connelly, W.E. Geiger, J. Am. Chem. Soc. 105 (1983) 2486;
 - (b) G.A. Lane, W.E. Geiger, N.G. Connelly, J. Am. Chem. Soc. 109 (1987) 2;
 - (c) A.J. Blake, R.O. Gould, T.I. Hyde, M. Schröder, J. Chem. Soc., Chem. Commun. (1987) 431;
 - (d) A.J. Blake, R.O. Gould, T.I. Hyde, M. Schröder, J. Chem. Soc., Chem. Commun. (1987) 1731;
 - (e) A.J. Blake, G. Reid, M. Schröder, J. Chem. Soc., Dalton Trans. (1990) 3363.
- [35] D.C. Powers, T. Ritter, Nat. Chem. 1 (2009) 302.
- [36] D.C. Powers, M.A.L. Geibel, J. Klein, T. Ritter, J. Am. Chem. Soc. 131 (2009) 17050.
- [37] N.R. Deprez, M.S. Sanford, J. Am. Chem. Soc. 131 (2009) 11234.
- [38] D.C. Powers, D. Benitez, E. Tkatchouk, W.A. Goddard III, T. Ritter, J. Am. Chem. Soc. 132 (2010) 14092.
- [39] D.C. Powers, T. Ritter, Top. Organomet. Chem. 35 (2011) 129.
- [40] S.H. Eitel, M. Bauer, D. Schweinfurth, N. Deibel, B. Sarkar, H. Kelm, H.-J. Kruger, W. Frey, R. Peters, J. Am. Chem. Soc. (2012), <http://dx.doi.org/10.1021/ja2098222>.
- [41] M.P. Lanci, M.S. Remy, W. Kaminsky, J.M. Mayer, M.S. Sanford, J. Am. Chem. Soc. 131 (2009) 15618.
- [42] J.R. Khusnutdinova, N.P. Rath, L.M. Mirica, J. Am. Chem. Soc. 132 (2010) 7303.
- [43] J.R. Khusnutdinova, N.P. Rath, L.M. Mirica, J. Am. Chem. Soc. 134 (2012) 2414.
- [44] L. Boisvert, M.C. Denney, H.S. Kloek, K.I. Goldberg, J. Am. Chem. Soc. 131 (2009) 15802.
- [45] G. Manolikakes, P. Knoche, Angew. Chem. Int. Ed. 48 (2009) 205.
- [46] J.R. Khusnutdinova, N.P. Rath, L.M. Mirica, Angew. Chem. Int. Ed. 50 (2011) 5532.
- [47] H.B. Gray, C.J. Ballhausen, J. Am. Chem. Soc. 85 (1963) 260.
- [48] N. Bartlett, P.R. Rao, Proc. Chem. Soc., Lond. (1964) 393.
- [49] A. Tressaud, M. Wintenberger, N. Bartlett, P. Hagenmuller, C. R. Acad. Sci. 282 (1976) 1069.
- [50] A.G. Sharpe, J. Chem. Soc. (1950) 3444.
- [51] R.S. Nyholm, A.G. Sharpe, J. Chem. Soc. (1952) 3579.
- [52] A. Tressaud, S. Khairoun, J.M. Dance, J. Grennec, G. Demazeau, P. Hagenmuller, C. R. Acad. Sci. 295 (1982) 183.
- [53] J.A. Weil, J.R. Bolton, J.E. Wertz, Electron Paramagnetic Resonance: Elementary Theory and Practical Applications, John Wiley & Sons, New York, NY, 1994.
- [54] A. Tressaud, S. Khairoun, J.M. Dance, J. Grennec, J. Portier, P. Hagenmuller, J. Fluorine Chem. 21 (1982) 28.
- [55] S. Khairoun, J.M. Dance, J. Grennec, G. Demazeau, A. Tressaud, Rev. Chim. Minér. 20 (1983) 871.
- [56] A. Tressaud, S. Khairoun, J.M. Dance, P. Hagenmuller, Z. Anorg. Allg. Chem. 517 (1984) 43.

- [57] A. Tressaud, S. Khairoun, J. Grennec, J.M. Dance, P. Hagenmuller, J. Fluorine Chem. 29 (1985) 39.
- [58] A. Tressaud, S. Khairoun, H. Touhara, N. Watanabe, P. Hagenmuller, Z. Anorg. Allg. Chem. 540 (1986) 291.
- [59] A.J. Blake, A.J. Holder, T.I. Hyde, M. Schröder, J. Chem. Soc., Chem. Commun. (1987) 987.
- [60] E. Stephen, A.J. Blake, E. Carter, D. Collison, E.S. Davies, R. Edge, W. Lewis, D.M. Murphy, C. Wilson, R.O. Gould, A.J. Holder, J. McMaster, M. Schröder, Inorg. Chem. ASAP (2012), <http://dx.doi.org/10.1021/ic2017006>.
- [61] A.J. Blake, L.M. Gordon, A.J. Holder, T.I. Hyde, G. Reid, M. Schröder, J. Chem. Soc., Chem. Commun. (1988) 1452.
- [62] A. McAuley, T.W. Whitcombe, Inorg. Chem. 27 (1988) 3090.
- [63] G. Reid, A.J. Blake, T.I. Hyde, M. Schröder, J. Chem. Soc., Chem. Commun. (1988) 1397.
- [64] A.J. Blake, G. Reid, M. Schröder, J. Chem. Soc., Dalton Trans. (1990) 3363.
- [65] A.J. Blake, R.D. Crofts, B. De Groot, M. Schröder, J. Chem. Soc., Dalton Trans. (1993) 485.
- [66] T. Krigas, M.T. Rogers, J. Chem. Phys. 54 (1971) 4769.
- [67] R.S. Eachus, R.E. Graves, J. Chem. Phys. 65 (1976) 5445.
- [68] N.V. Vugman, M.L.N. Grillo, V.K. Jain, Chem. Phys. Lett. 147 (1988) 241.
- [69] N.V. Vugman, M.L.N. Grillo, V.K. Jain, Chem. Phys. Lett. 188 (1992) 419.
- [70] A.S. Foust, R.H. Soderberg, J. Am. Chem. Soc. 89 (1967) 5507.
- [71] L.F. Warren Jr., M.F. Hawthorne, J. Am. Chem. Soc. 90 (1968) 4823.
- [72] A. Raizman, J. Barak, J.T. Suss, Phys. Rev. B: Condens. Matter 31 (1985) 5716.
- [73] V. Luca, R. Kukkadapu, L. Kevan, J. Chem. Soc., Faraday Trans. 87 (1991) 3083.
- [74] S.A. Jasper Jr., J.C. Huffman, L.J. Todd, Inorg. Chem. 37 (1998) 6060.
- [75] S.-J. Kim, S. Lemaux, G. Demazeau, J.-Y. Kim, J.-H. Choy, J. Am. Chem. Soc. 123 (2001) 10413.
- [76] A. Davison, N. Edelstein, R.H. Holm, A.H. Maki, J. Am. Chem. Soc. 85 (1963) 2029.
- [77] E. Hoyer, W. Dietzsch, H. Hennig, W. Schroth, Chem. Ber. 102 (1969) 603.
- [78] R. Kirmse, W. Dietzsch, J. Inorg. Nucl. Chem. 38 (1976) 255.
- [79] R. Kirmse, J. Stach, W. Dietzsch, G. Steimecke, E. Hoyer, Inorg. Chem. 19 (1980) 2679.
- [80] R. Kirmse, E. Moeller, C. Seitz, J. Reinhold, Z. Anorg. Allg. Chem. 623 (1997) 159.
- [81] E. Moeller, R. Kirmse, Inorg. Chim. Acta 257 (1997) 273.
- [82] A.L. Balch, R.H. Holm, J. Am. Chem. Soc. 88 (1966) 5201.
- [83] K. Ray, T. Weyhermueller, F. Neese, K. Wieghardt, Inorg. Chem. 44 (2005) 5345.
- [84] T. Motoyama, Y. Shimazaki, T. Yajima, Y. Nakabayashi, Y. Naruta, O. Yamauchi, J. Am. Chem. Soc. 126 (2004) 7378.
- [85] J.E. Sarneski, A.T. McPhail, K.D. Onan, L.E. Erickson, C.N. Reilley, J. Am. Chem. Soc. 99 (1977) 7376.
- [86] K. Wieghardt, M. Koeppen, W. Swiridoff, J. Weiss, J. Chem. Soc., Dalton Trans. (1983) 1869.
- [87] V.V. Rostovtsev, L.M. Henling, J.A. Labinger, J.E. Bercaw, Inorg. Chem. 41 (2002) 3608.
- [88] E. Stephen, D. Huang, J.L. Shaw, A.J. Blake, D. Collison, E.S. Davies, R. Edge, J.A.K. Howard, E.J.L. McInnes, C. Wilson, J. Wolowska, J. McMaster, M. Schröder, Chem. Eur. J. 17 (2011) 10246.
- [89] A.R. Dick, J.W. Kampf, M.S. Sanford, J. Am. Chem. Soc. 127 (2005) 12790.
- [90] F.A. Cotton, M. Matusz, R. Poli, X. Feng, J. Am. Chem. Soc. 110 (1988) 1144.
- [91] C.M. Che, L.Y. He, C.K. Poon, T.C.W. Mak, Inorg. Chem. 28 (1989) 3081.
- [92] H.-K. Yip, T.-F. Lai, C.-M. Che, Dalton Trans. (1991) 1639.
- [93] B.-H. Xia, C.-M. Che, Z.-Y. Zhou, Chem. Eur. J. 9 (2003) 3055.
- [94] S. Clement, S.M. Aly, D. Bellows, D. Fortin, C. Strohmann, L. Guyard, A.S. Abdel-Aziz, M. Knorr, P.D. Harvey, Inorg. Chem. 9 (2009) 4118.
- [95] J.E. Bercaw, A.C. Durrell, H.B. Gray, J.C. Green, N. Hazari, J.A. Labinger, J.R. Winkler, Inorg. Chem. 49 (2010) 1801.
- [96] D.L.M. Suess, J.C. Peters, Chem. Commun. 46 (2010) 6554.
- [97] N. Marino, C.H. Fazen, J.D. Blakemore, C.D. Incarvito, N. Hazari, R.P. Doyle, Inorg. Chem. 50 (2011) 2507.
- [98] J. Luo, J.R. Khusnutdinova, N.P. Rath, L.M. Mirica, Chem. Commun. 48 (2012) 1532.
- [99] K.R. Mann, J.G. Gordon, H.B. Gray, J. Am. Chem. Soc. 97 (1975) 3553.
- [100] I.V. Novozhilova, A.V. Volkov, P. Coppens, J. Am. Chem. Soc. 125 (2003) 1079.
- [101] Q.-J. Pan, H.-G. Fu, H.-T. Yu, H.-X. Zhang, Inorg. Chem. 45 (2006) 8729.
- [102] Q.-J. Pan, H.-X. Zhang, X. Zhou, H.-G. Fu, H.-T. Yu, J. Phys. Chem. A 111 (2007) 287.
- [103] F.A. Cotton, M. Matusz, R. Poli, Inorg. Chem. 26 (1987) 1472.
- [104] C.L. Yao, L.P. He, J.D. Korp, J.L. Bear, Inorg. Chem. 27 (1988) 4389.
- [105] J.F. Berry, E. Bill, E. Bothe, F.A. Cotton, N.S. Dalal, S.A. Ibragimov, N. Kaur, C.Y. Liu, C.A. Murillo, S. Nellutla, J.M. North, D. Villagran, J. Am. Chem. Soc. 129 (2007) 1393.
- [106] F.A. Cotton, J.D. Gu, C.A. Murillo, D.J. Timmons, J. Am. Chem. Soc. 120 (1998) 13280.
- [107] G.J. Chuang, W. Wang, E. Lee, T. Ritter, J. Am. Chem. Soc. 133 (2011) 1760.
- [108] F.A. Cotton, I.O. Koshevoy, P. Lahuerta, C.A. Murillo, M. Sanau, M.A. Ubeda, Q. Zhao, J. Am. Chem. Soc. 128 (2006) 13674.
- [109] D. Penno, V. Lillo, I.O. Koshevoy, M. Sanau, M.A. Ubeda, P. Lahuerta, E. Fernandez, Chem. Eur. J. 14 (2008) 10648.
- [110] D. Penno, F. Estevan, E. Fernandez, P. Hirva, P. Lahuerta, M. Sanau, M.A. Ubeda, Organometallics 30 (2011) 2083.
- [111] I. Ara, N. Chaouche, J. Forniés, C. Fortuño, A. Kribii, A.C. Tsipis, Organometallics 25 (2006) 1084.
- [112] M.G. Campbell, D.C. Powers, J. Raynaud, M.J. Graham, P. Xie, E. Lee, T. Ritter, Nat. Chem. 3 (2011) 949.
- [113] S. Takaishi, M. Takamura, T. Kajiwara, H. Miyasaka, M. Yamashita, M. Lwata, H. Matsuzaki, H. Okamoto, H. Tanaka, S. Kuroda, H. Nishikawa, H. Oshio, K. Kato, M. Takata, J. Am. Chem. Soc. 130 (2008) 12080.
- [114] M. Yamashita, S. Takaishi, Chem. Commun. 46 (2010) 4438.
- [115] B.S. Brunschwig, C. Creutz, N. Sutin, Chem. Soc. Rev. 31 (2002) 168.
- [116] K. Toriumi, Y. Wada, T. Mitani, S. Bandow, M. Yamashita, Y. Fujii, J. Am. Chem. Soc. 111 (1989) 2341.
- [117] S. Takaishi, H.S. Wu, J.X. Xie, T. Kajiwara, B.K. Breedlove, H. Miyasaka, M. Yamashita, Inorg. Chem. 49 (2010) 3694.
- [118] J.R. Khusnutdinova, L.M. Mirica, unpublished results.